symmetry

MDPI

Review

Localization Properties of Non-Periodic Electrical Transmission Lines

Edmundo Lazo

Departamento de Física, Facultad de Ciencias, Universidad de Tarapacá, Arica, Box 6-D, Chile; edmundolazon@gmail.com or elazo@academicos.uta.cl

Received: 7 September 2019; Accepted: 1 October 2019; Published: 9 October 2019

check for updates

Abstract: The properties of localization of the $I(\omega)$ electric current function in non-periodic electrical transmission lines have been intensively studied in the last decade. The electric components have been distributed in several forms: (a) aperiodic, including self-similar sequences (Fibonacci and m-tuplingtupling Thue–Morse), (b) incommensurate sequences (Aubry–André and Soukoulis–Economou), and (c) long-range correlated sequences (binary discrete and continuous). The localization properties of the transmission lines were measured using typical diagnostic tools of quantum mechanics like normalized localization length, transmission coefficient, average overlap amplitude, etc. As a result, it has been shown that the localization properties of the classic electric transmission lines are similar to the one-dimensional tight-binding quantum model, but also features some differences. Hence, it is worthwhile to continue investigating disordered transmission lines. To explore new localization behaviors, we are now studying two different problems, namely the model of interacting hanging cells (consisting of a finite number of dual or direct cells hanging in random positions in the transmission line), and the parity-time symmetry problem ($\mathcal{PT}$-symmetry), where resistances R_n are distributed according to gain-loss sequence ($R_{2n} = +R$, $R_{2n-1} = -R$). This review presents some of the most important results on the localization behavior of the $I(\omega)$ electric current function, in dual, direct, and mixed classic transmission lines, when the electrical components are distributed non-periodically.

Keywords: non-periodic systems; localization properties; electrical transmission lines

1. Introduction

Disordered one-dimensional quantum systems have been studied intensively since the pioneering work of Anderson [1]. It has been discovered that for one-dimensional uncorrelated disordered (random) systems, all states become localized states at the thermodynamic limit. Conversely, in periodic systems, all states are extended states, but for short-range or long-range correlated disorder, it is possible to find discrete sets or bands of extended states, respectively [2–29]. Also, these results have been verified experimentally [30–35]. In addition to correlated disordered systems, the fundamental properties of aperiodic systems have been extensively studied [36–74]. Aperiodic systems are formed by incommensurate systems and self-similar systems, and aperiodic incommensurate systems are generated by two superimposed periodic structures with incommensurate periods. The origin of incommensurability may be structural or dynamical. In the first case, there are two or more superimposed periodic structures whose periods are incommensurate, and in the second case one periodicity is related to the crystalline structure and the other to the behavior of elementary excitations that propagate through the crystal. On the other hand, self-similar systems are generated by specific substitutional rules.

After systematic studies of their properties, aperiodic systems can be classified based on two aspects: the spectral measures of their lattice Fourier transform and their Hamiltonian energy spectrum.

According to the Lebesgue's decomposition theorem, the energy spectrum of any measure in $\mathcal{R}^n$ can be uniquely decomposed into three types of spectral measures, namely (a) purely point spectra (μ_p), (b) absolutely continuous spectra (μ_{ac}) and (c) singularly continuous spectra (μ_{sc}). In addition, a combination of these measures is possible. Using spectral measures, Maciá [71,73] introduced a classification chart which includes periodic, amorphous and aperiodic systems. In this chart the abscissa is represented by the lattice Fourier transform and the ordinate is represented by the energy spectrum. In particular, we can see that the Fibonacci and the Thue–Morse systems share the same kind of singular continuous energy spectrum, known as a critical state. In this state, the wave function amplitude presents strong spatial fluctuations; however, the decaying envelope of the local maxima cannot be fitted to an exponential function, like the exponentially localized functions. On the other side, the spectral measure of the Fourier transform is different for these two self-similar systems, namely purely point spectra (μ_p) for Fibonacci systems, but singularly continuous spectra (μ_{sc}) for Thue–Morse systems. This way, the Fibonacci systems can be classified as quasi-periodic and the Thue–Morse systems are classified as aperiodic but not quasi-periodic. Despite this fundamental difference, most self-similar systems present an infinite number of gaps and consequently, the integrated density of states shows a fractal behavior. Also, the total bandwidth goes to zero in the thermodynamic limit $N \to \infty$.

This review presents recent results about the influence of the disordered distribution of electric components (capacitances and inductances) in the localization properties of dual, direct and mixed classical transmission lines (TL) [75–89]. To study the localization behavior of these non-periodic systems, the electric components have been distributed in a variety of forms: (a) aperiodic, including self-similar sequences (Fibonacci and $m-$tupling Thue–Morse), (b) incommensurate sequences (Aubry–André and Soukoulis–Economou), and (c) long-range correlated sequences (binary discrete and continuous). Although we are studying classical systems, the localization properties of the transmission lines are measured using the typical tools used in quantum mechanics to characterize the localization behavior of disordered systems. Specifically, we use the normalized localization length $\Lambda\,(\omega)$, the inverse participation ratio $IPR\,(\omega)$, the transmission coefficient $T\,(\omega)$, the global density of states $DOS\,(\omega)$, the average overlap amplitude C_ω, etc. Our studies indicate that the localization behavior of the classical electric transmission lines is similar to the one-dimensional tight-binding quantum model, but also displays some significant differences. Therefore it is important to keep investigating this type of classical disordered systems.

This review proceeds as follows. Section 2 describes the three ways to build classic electric transmission lines: dual, direct and mixed. Also, the allowed frequency spectrum for each kind of transmission line is calculated and, at the same time, the methods used to obtain the localization properties of these systems are described. Section 3 presents the localization behavior of transmission lines with different kinds of disorder, like aperiodic disorder and long-range correlated disorder. Section 4 shows the main results obtained so far in relation to the localization behavior of non-periodic electrical transmission lines. Also, a possible application to the study of electrical communication between neurons in included. Finally, two new lines of research to study the effect of the disorder on the localization properties of the electric current function are indicated.

2. Electric Transmission Lines

2.1. Direct and Dual Transmission Lines

We analyze ideal classical electric transmission lines considering three possible configurations, i.e., dual, direct, and mixed. We introduce the non-periodic disorder through the values of the inductances and capacitances of each cell of disordered TL [75–89].

Figure 1 shows a segment of a transmission line (dual or direct), with horizontal impedances denoted by Z_n and vertical impedances labeled γ_n. For direct TL the impedances are $Z_n = (i\omega L_n)$ and $\gamma_n = (i\omega C_n)^{-1}$, but for dual TL we have $Z_n = (i\omega C_n)^{-1}$ and $\gamma_n = (i\omega L_n)$. Here, C_n and L_n denote the capacitance and inductance values in cell n, respectively. To study the localization properties of the electric transmission lines, capacitances C_n, inductances L_n, or both are distributed using aperiodic sequences. Applying Kirchhoff's Loop Rule to three successive unit cells of the ideal TL shown in Figure 1, we obtain a linear relationship between the electric currents circulating in the $(n-1)$th, nth and $(n+1)$th cells.

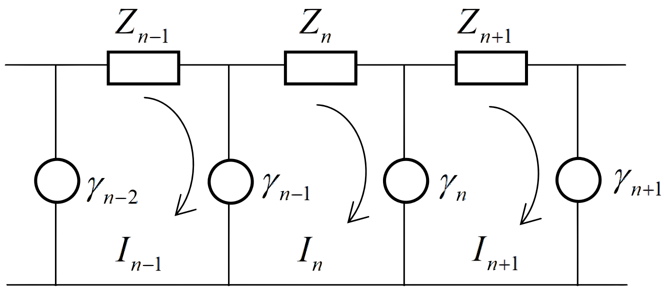

Figure 1. A partial view of an ideal transmission line. Z_n (γ_n) represent horizontal (vertical) impedances, respectively. For direct TL, Z_n is associated with inductances and γ_n with capacitances. Conversely, for dual TL, Z_n is associated with capacitances and γ_n with inductances. The arrows indicate the direction of the electric current in each cell. We arbitrarily consider the initial flow from the left, because we are using open boundary conditions

Specifically, for the direct transmission line, we find

$$\left(C_{n-1}^{-1} + C_n^{-1} - \omega^2 L_n\right) I_n - C_{n-1}^{-1} I_{n-1} - C_n^{-1} I_{n+1} = 0 \tag{1}$$

The corresponding equation for the dual TL, can be obtained using the following substitutions $\omega \to (\omega)^{-1}$, $C_n \to (L_n)^{-1}$, $L_n \to (C_n)^{-1}$, namely

$$\left(L_{n-1} + L_n - \left(\omega^2 C_n\right)^{-1}\right) I_n - L_{n-1} I_{n-1} - L_n I_{n+1} = 0 \tag{2}$$

In both cases, Equations (1) and (2) can be put in a simple generic form

$$D_n I_n - B_{n-1} I_{n-1} - B_n I_{n+1} = 0 \tag{3}$$

where

$$D_n = (B_{n-1} + B_n - A_n) \tag{4}$$

Notice that A_n always depends on frequency ω and the values of capacitances C_n or inductances L_n, while B_n only depends on C_n or L_n. To be specific, for direct TL we have $A_n = \omega^2 L_n$ and $B_n = C_n^{-1}$, but for dual TL we have $A_n = \left(\omega^2 C_n\right)^{-1}$ and $B_n = L_n$. Please note that when we introduce disorder in the off-diagonal terms, this disorder simultaneously appears in the diagonal term D_n.

2.2. Mixed Transmission Lines

The spectrum of allowed frequencies of periodic dual and direct transmission lines contains a single band. To obtain a frequency spectrum with more bands, namely a frequency selector, recently a combination of dual and direct cells, called mixed transmission line, has been studied. [87,88]. These electric systems are formed by a basic unit of $d = (p+q)$ cells consisting of a set of p successive direct cells followed by q successive dual cells. The N total number of cells in the mixed TL is given by $N = d\,N_s$, where N_s is the number of times we repeat the basic unit. Figure 2 shows a segment of a mixed TL with $p = 2$, $q = 3$ and $d = 5$. Applying Kirchhoff's Loop Rule to this system, we find a set of equations similar to Equations (1) and (2). Consequently, equations describing mixed transmission lines can also be written in the same form as the generic Equation (3), but now both coefficients D_n and B_n usually depend on the frequency ω, the parameters p, q and capacitances $C_{n,x}$, $C_{n,y}$, and inductances

$L_{n,x}$, $L_{n,y}$, corresponding to direct and dual cells, respectively. Consequently, mixed TL contain a richer parameter space to study the localization properties of the $I\left(\omega\right)$ electric current function. This allows obtaining exactly $d = (p + q)$ bands separated by gaps, containing extended and localized states and even gaps. In this way, the mixed transmission line becomes a frequency selector.

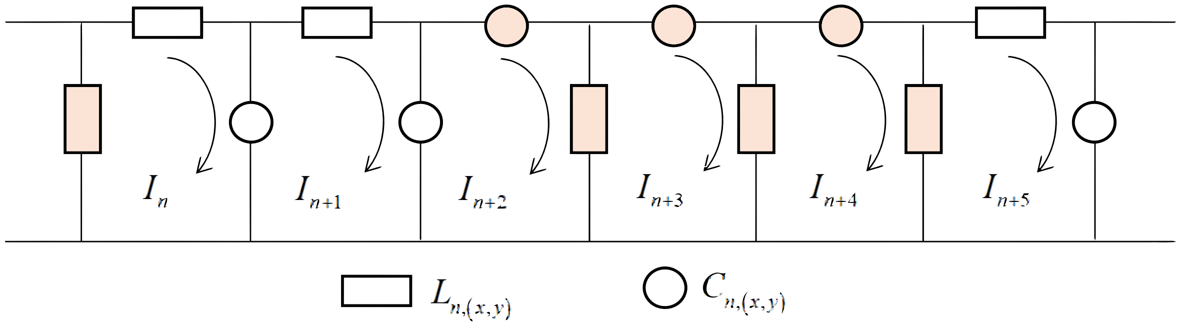

Figure 2. A segment of a mixed transmission line formed by $p = 2$ direct cells and $q = 3$ dual cells. The full system is formed by the repetition of the basic unit formed by $d = (p + q)$ cells. Inductances are represented by rectangles and capacitances by circles. In addition, dual cells are marked with orange color-filled symbols. The arrows indicate the direction of the electric current in each cell.

2.3. Relation with the Tight-Binding Model

The generic Equation (3) describing the relationship between three consecutive electric current amplitudes $I_{n-1}\left(\omega\right)$, $I_n\left(\omega\right)$ and $I_{n+1}\left(\omega\right)$ in the classical electrical transmission lines, has the same form that the equation describing the relationship between three consecutive amplitudes $\phi_{n-1}\left(E\right)$, $\phi_n\left(E\right)$ and $\phi_{n+1}\left(E\right)$ of the wave function of the one-dimensional tight-binding quantum model. This correspondence has allowed to test the effects of the disorder in one-dimensional quantum systems using classical electrical circuits with random distribution of capacitances and inductances. Consequently, Equation (3) can be mapped to the quantum one-dimensional tight-binding model

$$\left(E - \varepsilon_n\right)\phi_n - V_{n-1}\phi_{n-1} - V_n\phi_{n+1} = 0 \tag{5}$$

where ε_n is the site energy, V_n the hopping between neighboring sites, E the eigenenergy, and ϕ_n is the eigenfunction. In this quantum model, it is always possible to study separately the diagonal disordered case and the off-diagonal disordered case. However, in classical electrical TL, indicated by relations (1) and (2), the introduction of disorder in the off-diagonal terms necessarily implies that the disorder appears in both the diagonal and off-diagonal terms. Nonetheless, a correspondence between the tight-binding Equation (5) and Equations (1) and (2) exists. Applying the following transformation in the tight-binding Equation (5) we obtain the direct TL (1),

$$E = -\omega^2, \quad \varepsilon_n = -L_n^{-1}\left(C_{n-1}^{-1} + C_n^{-1}\right), \quad \phi_n = I_n\left(L_n\right)^{-\frac{1}{2}} \tag{6}$$

$$V_{n-1} = C_{n-1}^{-1}\left(L_{n-1}L_n\right)^{-\frac{1}{2}}, \quad V_n = C_n^{-1}\left(L_nL_{n+1}\right)^{-\frac{1}{2}} \tag{7}$$

To obtain the dual TL (2) from the tight-binding equation, it suffices to do the following changes in transformations (6) and (7), that is $\omega \rightarrow \left(\omega\right)^{-1}$, $C_n \rightarrow \left(L_n\right)^{-1}$, $L_n \rightarrow \left(C_n\right)^{-1}$. This correspondence between the tight-binding quantum model and the classical transmission lines allows checking the localization behavior of quantum disordered one-dimensional systems using disordered TL.

2.4. Spectrum of Allowed Frequencies

To obtain the spectrum of allowed frequencies of dual and direct TL, the generic Equation (3), $D_nI_n - B_{n-1}I_{n-1} - B_nI_{n+1} = 0$, can be written in the following form:

$$I_{n+1} = \frac{D_n}{B_n} I_n - \frac{B_{n-1}}{B_n} I_{n-1} \tag{8}$$

Considering the trivial relation $I_n = I_n$, we obtain a map in the plane (I_n, I_{n+1})

$$\begin{pmatrix} I_{n+1} \\ I_n \end{pmatrix} = M_n \begin{pmatrix} I_n \\ I_{n-1} \end{pmatrix} \tag{9}$$

where matrix M_n is given by

$$M_n = \begin{pmatrix} \frac{D_n}{B_n} & -\frac{B_{n-1}}{B_n} \\ 1 & 0 \end{pmatrix} \tag{10}$$

The trajectories of the map (9) can be used to determine the extended or localized character of the electric current function $I_n(\omega)$, i.e., for extended states the trajectories are bounded, but unbounded for localized states. Also, the λ_n eigenvalues of the M_n matrix can be written in the following complex form:

$$\lambda_n = \frac{D_n}{2B_n} \pm i \sqrt{\frac{B_{n-1}}{B_n} - \left(\frac{D_n}{2B_n}\right)^2} \tag{11}$$

For a given frequency ω, the map (9) is stable if the eigenvalues λ_n of the matrix M_n are complex numbers, which also implies that the trajectories of the map are bounded, which in turn means that the electric current $I_n(\omega)$ is an extended function. λ_n is a complex number if condition $\left(\frac{B_{n-1}}{B_n}\right) > \left(\frac{D_n}{2B_n}\right)^2$ is met. For $\left(\frac{B_{n-1}}{B_n}\right) = \left(\frac{D_n}{2B_n}\right)^2$ we find the separatrix between localized states $\left(\left(\frac{B_{n-1}}{B_n}\right) < \left(\frac{D_n}{2B_n}\right)^2\right)$ and extended states. Consequently, the spectrum of allowed frequencies for direct and dual TL is given by general condition

$$\left(\sqrt{B_n} - \sqrt{B_{n-1}}\right) < \sqrt{A_n} < \left(\sqrt{B_n} + \sqrt{B_{n-1}}\right) \tag{12}$$

The coefficients A_n and B_n depend on the type of transmission line considered, direct or dual. For direct TL we have $B_n = C_n^{-1}$ and $A_n = \omega^2 L_n$ and the allowed frequencies are given by

$$\left((L_n C_n)^{-\frac{1}{2}} - (L_n C_{n-1})^{-\frac{1}{2}}\right) < \omega < \left((L_n C_n)^{-\frac{1}{2}} + (L_n C_{n-1})^{-\frac{1}{2}}\right) \tag{13}$$

For pure direct TL with $L_n = L_0$, $C_n = C_0$, $\forall n$, we find the typical band of frequencies, i.e., $0 < \omega < \frac{2}{\sqrt{L_0 C_0}}$. Conversely, for dual TL we have $B_n = L_n$ and $A_n = \left(\omega^2 C_n\right)^{-1}$ and the allowed frequencies are

$$\left(\sqrt{C_n L_n} + \sqrt{C_n L_{n-1}}\right)^{-1} < \omega < \left(\sqrt{C_n L_n} - \sqrt{C_n L_{n-1}}\right)^{-1} \tag{14}$$

For pure dual TL with $L_n = L_0$, $C_n = C_0$, $\forall n$, we also find the typical band of frequencies, i.e., $\frac{1}{2\sqrt{L_0 C_0}} < \omega < \infty$.

Next, we determined the frequency spectrum allowed for mixed transmission lines with p direct cells and q dual cells in the basic unit. The frequency spectrum shows a set of $d = (p+q)$ allowed bands separated by gaps in a bounded region of frequencies. The size and position of these d bands depends on the set of parameters that define the mixed TL, namely p, q, and the values of capacitances $C_{n,x}$, $C_{n,y}$, and inductances $L_{n,x}$, $L_{n,y}$ in direct or dual cell, respectively. Using the generic Equation (3) we write the relationship between three consecutive cells of the mixed TL. Starting from the first site with index n belonging to the direct type cell, we write p equations. After that we write q equations corresponding to dual cells. We repeat this process until we generate the complete mixed TL. Using a matrix decimation process [90,91] we can eliminate equations with sites between $(n+1)$

and $(n+d-1)$, and between $(n+d+1)$ and $(n+2d-1)$ and so on. This process allows us to write a new generic equation with renormalized coefficients D^R_{n+jd} and B^R_{n+jd}, which connects sites that are separated by a distance d, namely

$$D^R_{n+jd} I_{n+jd} - B^R_{n+(j-1)d} I_{n+(j-1)d} - B^R_{n+jd} I_{n+(j+1)d} = 0 \tag{15}$$

where $j = 0, 1, 2, 3, \ldots$ Studying bounded trajectories of the new renormalized map, we obtain the spectrum of allowed frequencies for mixed TL, i.e.,

$$\left| D^R_{n+jd} \right| < 2\sqrt{B^R_{n+(j-1)d} B^R_{n+jd}} \tag{16}$$

From this relationship, two algebraic inequations of degree d in the variable ω^2 are found. Solving both inequations, exactly $d = (p+q)$ bands are obtained, within which we can observe extended and localized states, and even gaps. The size and position of these $d = (p+q)$ bands depends on the number of direct cells p and the number of dual cells q that form the mixed TL, as well as on the values of capacitances $C_{n,x}$, $C_{n,y}$ and inductances $L_{n,x}$, $L_{n,y}$ of direct and dual cells, respectively.

2.5. Methods to Obtain the $I_n(\omega)$ Electric Current Function

The $I_n(\omega)$ amplitudes of the electric current function, are obtained solving the generic Equation (3). In this paper we only consider two methods to solve this equation: (a) the recurrence method and (b) The Hamiltonian map method.

2.5.1. Recurrence Method

The $I_n(\omega)$ electric current amplitude in each cell, can be calculated using the following method. First, the generic Equation (3) is divided by I_n and then γ_n is defined as follows

$$\gamma_n = \left(B_n \frac{I_{n+1}}{I_n} \right) \tag{17}$$

Then, Equation (3) is transformed into a recurrence equation for γ_n,

$$\gamma_n = D_n - \frac{1}{\gamma_{n-1}} (B_{n-1})^2 \tag{18}$$

where $2 \leq n \leq N$. Iterating this equation, and starting with $\gamma_1 = D_1 = (B_1 - A_1)$, the full set of γ_n values, with $n = 1, 2, 3, \ldots, N$ is obtained. With these γ_n values, and using an arbitrary initial amplitude value $I_1 = 1$, the full set of amplitudes $\{I_n\}$ of the electric current function, can be calculated, i.e.,

$$I_{n+1} = \left(\frac{\gamma_n}{B_n} \right) I_n \tag{19}$$

with $1 \leq n \leq (N-1)$. After that, the electric current function is normalized, i.e., $\sum_{n=1}^{N} |I_n|^2 = 1$.

Exactly the same procedure can be applied to calculate $\{I_n\}$ for mixed transmission lines, because the coefficients γ_n are always defined from the generic Equation (3), so it is not necessary to use the renormalized generic Equation (15). Also, the same is valid for the Hamiltonian map method.

2.5.2. Hamiltonian Map Method

Starting from the generic Equation (3), $D_n I_n - B_{n-1} I_{n-1} - B_n I_{n+1} = 0$, we are building a two-dimensional map (the Hamiltonian map) [28,81,83,87,88]. From the study of this map we will obtain (a) the full set of electric current amplitudes $\{I_n\}$ (from which we will obtain the localization properties) and (b) the $T(\omega)$ transmission coefficient of the disordered TL (a crucial localization tool).

Using electric current amplitudes I_n, we define the coordinate x_n at cell n, and the momentum p_n (Hamiltonian description) in the following form:

$$\begin{aligned} x_n &= I_n \\ p_n &= B_{n-1}\left(I_n - I_{n-1}\right) \end{aligned} \tag{20}$$

The generic Equation (3) can also be written using the coordinate x_n,

$$D_n x_n - B_{n-1}x_{n-1} - B_n x_{n+1} = 0 \tag{21}$$

with $D_n = \left(B_{n-1} + B_n - A_n\right)$. After some algebra, we obtain the Hamiltonian map as a function of the coefficient A_n, α_n and β_n

$$\begin{aligned} x_{n+1} &= \alpha_n x_n + \beta_n p_n \\ p_{n+1} &= -A_n x_n + p_n \end{aligned} \tag{22}$$

where for simplicity we have defined $\beta_n = \left(\frac{1}{B_n}\right)$ and $\alpha_n = (1 - A_n\beta_n)$. This map can be written as $Z_{n+1} = M_n\, Z_n$, where $Z_{n+1} = \begin{pmatrix} x_{n+1} & p_{n+1} \end{pmatrix}^{\tau}$ and M_n is given by

$$M_n = \begin{pmatrix} \alpha_n & \beta_n \\ -A_n & 1 \end{pmatrix} \tag{23}$$

The trajectories of this map in the phase space (x, p) determine the localization properties of the $I_n\,(\omega)$ electric current amplitudes, namely for bounded trajectories $I_n\,(\omega)$ is an extended function, but for unbounded trajectories $I_n\,(\omega)$ is a localized function. Importantly, the study of the map's evolution (22) at "time" n, is similar to the transfer matrix method [5,28] used to study the localization behavior of disordered systems. On the other hand, starting from this map, the spectrum of allowed frequencies we can be calculated studying the complex eigenvalues of the Hamiltonian matrix M_n (see Section 2.4).

Next, variables (x, p) of the map (22) are changed by the canonical variables (r, θ) in the following way

$$x = r\sin\theta \tag{24}$$

$$p = r\cos\theta \tag{25}$$

Using (24) and (25) the map (22) becomes

$$r_{n+1}\sin\theta_{n+1} = \alpha_n r_n \sin\theta_n + \beta_n r_n \cos\theta_n \tag{26}$$

$$r_{n+1}\cos\theta_{n+1} = -A_n r_n \sin\theta_n + r_n\cos\theta_n \tag{27}$$

Dividing Equation (26) by Equation (27) we obtain a recurrence equation from which we can calculate θ_{n+1} as a function of θ_n, namely

$$\tan\theta_{n+1} = \frac{\beta_n + \alpha_n\tan\theta_n}{1 - A_n\tan\theta_n} \tag{28}$$

Now, squaring Equations (26) and (27) and adding them together, we have

$$\left(\frac{r_{n+1}}{r_n}\right)^2 = \left(\alpha_n^2 + A_n^2\right)\sin^2\theta_n + \left(\beta_n^2 + 1\right)\cos^2\theta_n + \left(\alpha_n\beta_n - A_n\right)\sin 2\theta_n \tag{29}$$

Defining Γ_n as

$$\Gamma_n = \frac{r_{n+1}}{r_n} \tag{30}$$

the recurrence equation to calculate r_{n+1} as a function of r_n, is as follows

$$r_{n+1} = r_n \Gamma_n \tag{31}$$

In this way, for a fixed frequency ω, and starting with an initial condition (r_0, θ_0), the full set of values of θ_n and r_n. can be obtained. Then, using $I_n = x_n$ and $x_n = r_n \sin\theta_n$, we can calculate the following relationship

$$\frac{I_{n+1}}{I_n} = \frac{x_{n+1}}{x_n} = \frac{r_{n+1}\sin\theta_{n+1}}{r_n \sin\theta_n} = \Gamma_n \left(\frac{\sin\theta_{n+1}}{\sin\theta_n}\right) \tag{32}$$

from which we obtain the recurrence relation to calculate all electric current amplitudes I_n, as a function of Γ_n and θ_n, namely

$$I_{n+1} = \Gamma_n \left(\frac{\sin\theta_{n+1}}{\sin\theta_n}\right) I_n \tag{33}$$

where $1 \le n \le (N-1)$.

2.6. Diagnostic Tools

Diagnostic tools have been introduced in the literature to study disordered quantum systems, because the Bloch theorem cannot be applied in the non-periodic case. To accurately estimate the degree of localization of the quantum wave function, it is generally necessary to simultaneously apply two or more different diagnostic tools. It is important to note that these diagnostic tools also allow us to determine the localization properties of classical systems, such as harmonic chains and electric transmission lines.

2.6.1. Usual Diagnostic Tools

To study the localization behavior of the disordered electric TL as a function of the frequency ω and as a function of the kind and degree of disorder, we deploy tools used in the study of the localization behavior of quantum systems: the Lyapunov exponent $\lambda(\omega)$, the normalized localization length $\Lambda(\omega)$, the participation number $D(\omega)$, the inverse participation ratio $IPR(\omega)$, the global density of states $DOS(\omega)$ and the transmission coefficient $T(\omega)$. In addition, to characterize the localization behavior of disordered TL, we study the $R_q(\omega)$ Rényi entropies [92] and the moments $\mu_q(\omega)$. All localization tools are defined as a function of the normalized electric current amplitude $I_n(\omega)$, namely $\sum_{n=1}^{N} |I_n(\omega)|^2 = 1$. In the quantum case, the localization properties are measured using the $\phi_n(E)$ amplitude of the normalized quantum wave function.

The $\lambda(\omega)$ Lyapunov exponent is defined as

$$\lambda(\omega) = \lim_{N\to\infty} \frac{1}{N} \sum_{n=1}^{N} \ln\left|\frac{I_{n+1}}{I_n}\right| \tag{34}$$

For extended states the following condition is met: $\lambda(\omega) \le \frac{1}{N}$. From (34) we define the $Loc(\omega)$ localization length as $Loc(\omega) = \lambda^{-1}(\omega)$. Then, the $\Lambda(\omega)$ normalized localization length is defined as

$$\Lambda(\omega) = \frac{Loc(\omega)}{N} = (N\lambda(\omega))^{-1} \tag{35}$$

For extended states we have $\Lambda(\omega) \ge 1$ and for localized states we obtain $\Lambda(\omega) < 1$.

Next, we considered the $\mu_q(\omega)$ moments of the $I_n(\omega)$ electric current function. Given that we are working with normalized electric current $\sum_{n=1}^{N} |I_n|^2 = 1$, we can define the moments $\mu_q(\omega)$ in the following form

$$\mu_q(\omega) = \sum_{n=1}^{N} |I_n|^{2q} \tag{36}$$

For homogeneous distribution of $I_n(\omega)$, i.e., for $I_n(\omega) = \frac{1}{\sqrt{N}}$, $\forall n$, we find $\mu_q(\omega) = N^{-(q-1)}$. This case corresponds to the most extended case. Conversely, for fully localized states in which $I_n(\omega) = \delta_{n,m}$, we obtain $\mu_q(\omega) = 1$. The participation number $D(\omega)$ can be defined using $\mu_2(\omega)$ namely

$$D(\omega) = \frac{1}{\mu_2} = \left(\sum_{n=1}^{N} |I_n|^4\right)^{-1} \tag{37}$$

with $1 \le D(\omega) \le N$. For extended states, $D(\omega)$ scales proportional to the N system size, which implies that $\ln(D(\omega))$ versus $\ln(N)$ is a straight line with slope m approximate to $m = 1$. Also, we can define the $\xi(\omega)$ normalized participation number as $\xi(\omega) = \frac{D(\omega)}{N}$, with $\frac{1}{N} \le \xi(\omega) \le 1$. Consequently, for extended states, $\xi(\omega)$ tends to a constant value as a function of N. In particular, for periodic systems $\xi(\omega) = \left(\frac{2}{3}\right)$. Conversely, for localized states $\xi(\omega) \to 0$. In addition, the moment μ_2 is known as the inverse participation ratio $IPR(\omega) = \mu_2 = D^{-1}(\omega)$. Consequently, $\frac{1}{N} < IPR(\omega) \le 1$. Sometimes it is useful to calculate $(N \times IPR)$. In this case, for localized states $(N \times IPR) \to N$ and for extended states $(N \times IPR) \approx 1$. In particular, for the most extended case $(N \times IPR) = \left(\frac{3}{2}\right)$. Notice that $\xi(\omega) = (N \times IPR)^{-1}$.

Also, some of these magnitudes can be obtained as a special case of the $R_q(\omega)$ Rényi entropies [92] defined as

$$R_q(\omega) = \frac{1}{1-q} \ln \sum_{n=1}^{N} |I_n|^{2q}, \quad q \ne 1 \tag{38}$$

In the limit $q \to 1$ we obtain the Shannon entropy ($S(\omega) = \lim_{q\to 1} R_q(\omega) = R_1$)

$$S(\omega) = -\sum_{n=1}^{N} |I_n|^2 \ln |I_n|^2 \tag{39}$$

For $q = 2$ we find $R_2(\omega) = \ln D = -\ln IPR$. Moreover, the Rényi entropies $R_q(\omega)$ can be defined using the $\mu_q(\omega)$ moments in the following form

$$R_q(\omega) = \frac{1}{1-q} \ln \mu_q(\omega), \quad q \ne 1 \tag{40}$$

2.6.2. The Average Overlap Amplitude C_ω

Another tool recently introduced in the literature is the C_{ij}^{ω} overlap amplitude [84,86–88]. For fixed frequency ω, this quantity measures the overlap between electric current amplitudes $I_i(\omega)$ and $I_j(\omega)$, corresponding to two cells i and j of the TL and is defined as $C_{ij}^{\omega} = 2\left|I_i(\omega) I_j(\omega)\right|$. For homogeneous distribution of $I_j(\omega)$, i.e., for $I_j(\omega) = \frac{1}{\sqrt{N}}$, $\forall j$, we find $C_{ij}^{\omega} = \frac{2}{N}$. This case corresponds to the most extended case. On the contrary, for fully localized states such as $I_j(\omega) = \delta_{i,j}$, we obtain $C_{ij}^{\omega} = 0$. Given that C_{ij}^{ω} depends on each pair of sites i and j, we define the average overlap amplitude $C_\omega = \left\langle C_{ij}^{\omega} \right\rangle$ considering all cells of the TL, namely

$$C_\omega = \left\langle C_{ij}^{\omega} \right\rangle = \frac{1}{d} \sum_{i<j} C_{ij}^{\omega} \tag{41}$$

where $d = \frac{1}{2}N\left(N-1\right)$. The overlap amplitude is based on the definition of quantum entanglements between a pair of qubits, i and j, called pairwise entanglement (pairwise concurrence) [93,94].

Next, we considered the power of $2q$ of the overlap amplitude, C_{ij}^{ω}, i.e.,

$$\left(C_{ij}^{\omega}\right)^{2q} = 2^{2q}\left|I_i\left(\omega\right)I_j\left(\omega\right)\right|^{2q} \tag{42}$$

The average of this quantity over all cells of the TL, is given by

$$\left\langle\left(C_{ij}^{\omega}\right)^{2q}\right\rangle = \frac{2^{2q}}{d}\sum_{i<j}\left|I_i\left(\omega\right)\right|^{2q}\left|I_j\left(\omega\right)\right|^{2q} \tag{43}$$

After some algebra [84], this expression can be written as a function of the μ_q moments (36) of the electric current function, namely

$$\left\langle\left(C_{ij}^{\omega}\right)^{2q}\right\rangle = \frac{2^{2q-1}}{d}\left(\left(\mu_q\right)^2 - \mu_{2q}\right) \tag{44}$$

This relationship indicates that $\left\langle\left(C_{ij}^{\omega}\right)^{2q}\right\rangle$ can determine the localization degree for any disordered system. For the case $q = \frac{1}{2}$, we obtain a simple expression to calculate the average overlap amplitude C_{ω}, i.e.,

$$C_{\omega} = \left\langle C_{ij}^{\omega}\right\rangle = \frac{1}{d}\left\{\left(\sum_{n=1}^{N}\left|I_n\right|\right)^2 - 1\right\} \tag{45}$$

Also, for $q = 1$, $\left\langle\left(C_{ij}^{\omega}\right)^{2}\right\rangle$ can be calculated as a function of the $\xi\left(\omega\right)$ normalized participation number [84,95],

$$\left\langle\left(C_{ij}^{\omega}\right)^{2}\right\rangle = \frac{2}{d}\left\{1 - \frac{1}{N\xi\left(\omega\right)}\right\} \tag{46}$$

For localized states $\xi\left(\omega\right) \to \frac{1}{N}$, which implies that $\left\langle\left(C_{ij}^{\omega}\right)^{2}\right\rangle \to 0$. Conversely, for extended states $\xi\left(\omega\right) \to 1$, then $\left\langle\left(C_{ij}^{\omega}\right)^{2}\right\rangle = \left(\frac{2}{N}\right)^2$.

In general, for any value of q, for homogeneous extended states, the following scaling relationship is obtained

$$\left\langle\left(C_{ij}^{\omega}\right)^{2q}\right\rangle = \left(\frac{2}{N}\right)^{2q} \tag{47}$$

but for fully localized states, we find $\left\langle\left(C_{ij}^{\omega}\right)^{2q}\right\rangle = 0$. In particular, for $q = \frac{1}{2}$, we find that $\left(N\left\langle C_{ij}^{\omega}\right\rangle\right)$ scales like $\left(NC_{\omega}\right) \to 2$, which means that for extended states, $\left(NC_{\omega}\right)$ is independent of system size N.

In this way, the average overlap amplitude and its powers $\left\langle\left(C_{ij}^{\omega}\right)^{2q}\right\rangle$ can adequately determine the degree of localization of the disordered TL. Finally, $\left\langle\left(C_{ij}^{\omega}\right)^{2q}\right\rangle$ can also be expressed as a function of the Rényi entropies [84,95]

$$\left\langle\left(C_{ij}^{\omega}\right)^{2q}\right\rangle = \frac{2^{2q-1}}{d}\left\{\left(e^{R_q}\right)^{2(1-q)} - \left(e^{R_{2q}}\right)^{(1-2q)}\right\} \tag{48}$$

The results shown in this subsubsection are valid even for the quantum case, considering that C_{ij}^{ω} represents the quantum entanglements between a pair of qubits C_{ij}^{E}, i and j, called pairwise entanglement (pairwise concurrence) [93,94], i.e., $C_{ij}^{E} = 2\left|\phi_i(E)\,\phi_j(E)\right|$, where $\phi_j(E)$ represents the amplitude of the quantum wave function for the eigenstate with eigenenergy E.

2.6.3. The Transmission Coefficient T_ω

To study the transmission properties of disordered TL using the Hamiltonian map (22), the disordered segment must be embedded in two semi-infinite ordered TL, in a similar way to the transfer matrix method [5,28]. From the Hamiltonian map formalism discussed above, the transmission coefficient $T(\omega)$ can be calculated from the expression [5,28,81,83]

$$T(\omega) = \frac{2}{1+Z_N} \tag{49}$$

For bounded trajectories of the Hamiltonian map (22), we have $Z_N \to 1$ and $T(\omega) \to 1$. This behavior indicates that the electric current function $I(\omega)$ is an extended function. On the contrary, for unbounded trajectories we have $Z_N \to \infty$ and $T(\omega) \to 0$. In this case, $I(\omega)$ is a localized function. Z_N is defined as

$$Z_N = \frac{1}{2}\left(\left(r_N^{(1)}\right)^2 + \left(r_N^{(2)}\right)^2\right) \tag{50}$$

where $r_N^{(1,2)}$ are the radii of two trajectories at "time" $n = N$ that start from two perpendicular initial points, i.e.,

$$\begin{aligned} \left(r_0^{(1)}, \theta_0^{(1)}\right) &= (1, 0) \\ \left(r_0^{(2)}, \theta_0^{(2)}\right) &= \left(1, \frac{\pi}{2}\right) \end{aligned} \tag{51}$$

The radii $r_N^{(1,2)}$ can be calculated using the relationship (31), i.e., $r_{n+1} = r_n\Gamma_n$, then $\left(r_N^{(j)}\right)^2$ is given by

$$\left(r_N^{(j)}\right)^2 = \prod_{n=1}^{N}\left(\Gamma_n^{(j)}\right)^2, \quad j = 1, 2 \tag{52}$$

Or in another form

$$\left(r_N^{(j)}\right)^2 = \exp\left(2\sum_{n=1}^{N}\ln\left(\Gamma_n^{(j)}\right)\right), \quad j = 1, 2 \tag{53}$$

Therefore, Z_N is given by

$$Z_N = \frac{1}{2}\left[\exp\left(2\sum_{n=1}^{N}\ln\left(\Gamma_n^{(1)}\right)\right) + \exp\left(2\sum_{n=1}^{N}\ln\left(\Gamma_n^{(2)}\right)\right)\right] \tag{54}$$

In this way we have a procedure to calculate the transmission coefficient $T(\omega)$.

3. Disordered Transmission Lines

In this section, we study the localization behavior of the $I(\omega)$ electric current function when we distribute capacitances and inductances in a non-periodic way in dual, direct and mixed transmission lines. Here we will consider (a) aperiodic systems formed by self-similar sequences and incommensurate sequences, and (b) long-range correlated sequences. The general results indicate that the band structure of non-periodic systems is determined by the type of transmission line (dual, direct or mixed) in which the disorder is introduced, and that the existence of discrete sets or extended state bands in the thermodynamic limit, it depends on the type of aperiodic disorder used to distribute the electrical components.

3.1. Aperiodic Transmission Lines

3.1.1. Generalized Fibonacci Sequence

The generalized Fibonacci quasi-periodic sequence is given by substitution rule $A \to A^m B^n$, $B \to A$. The corresponding substitution matrix M is given by

$$M = \begin{bmatrix} m & n \\ 1 & 0 \end{bmatrix} \tag{55}$$

where the elements of the substitution matrix indicate the number of times a given letter, A or B, appears in the substitution rule, without considering the order in which these letters occur. The number of letters that appear after applying the substitution rule j times, is given by the generalized Fibonacci numbers F_j, namely $F_j = mF_{j-1} + nF_{j-2}$, $j \geq 2$, with $F_0 = F_1 = 1$. When the number of iterations j goes to infinity, the ratio between two consecutive Fibonacci numbers F_j and F_{j-1} tends to a constant number $\sigma_{m,n}$ called the mean of incommensurability, i.e.,

$$\sigma_{m,n} = \lim_{j\to\infty}\left(\frac{F_j}{F_{j-1}}\right) = \frac{1}{2}\left(m + \sqrt{m^2+4n}\right) \tag{56}$$

In addition, the relative frequency of both types of letters $n_A = \frac{N_A}{N}$ and $n_B = \frac{N_B}{N}$ in the limit $j \to \infty$ is given by $n_A = \frac{\sigma_{m,n}}{\sigma_{m,n}+n}$ and $n_B = \frac{n}{\sigma_{m,n}+n}$. Please note that the mean of incommensurability $\sigma_{m,n}$ can also be obtained as the maximal eigenvalue $\lambda = \sigma_{m,n}$ of the substitution matrix M (55). For the case $m = 1$ and $n = 1$, we obtain the golden mean $\sigma_{1,1} = \frac{1}{2}\left(1+\sqrt{5}\right)$, and the corresponding Fibonacci sequence is the following:

$$A \to AB \to ABA \to ABAAB \to ABAABABA \to \cdots$$

Some of the other Fibonacci means [71,73,74] which have been studied are: the Silver mean $\sigma_{2,1} = \left(1+\sqrt{2}\right)$, the Copper mean $\sigma_{1,2} = 2$, the Bronze mean $\sigma_{3,1} = \frac{1}{2}\left(3+\sqrt{13}\right)$, the Nickel mean $\sigma_{1,3} = \frac{1}{2}\left(1+\sqrt{13}\right)$, etc. See Maciá [73] for a spectral classification of one-dimensional binary aperiodic crystals, studying the eigenvalues $\lambda_{\pm}$ and the determinant $|M|$ of the substitution matrix M.

The Fibonacci tight-binding quantum disordered systems have been studied exhaustively by [37,38,40–46,59,60,63,71]. For the diagonal disordered case, the global number of sub-bands is exactly four. However, in the off-diagonal disordered case, the global number of sub-bands is exactly three. In both cases, each sub-band is divided into three sub-bands until it is resolvable. This self-replication behavior is characteristic of quasi-periodic systems. On the other hand, in classical electric systems, dual and mixed transmission lines have been studied [78,87] using a Fibonacci distribution of two different values of inductances L_A and L_B, namely

$$L_A L_B L_A L_A L_B L_A L_B L_A L_A L_B L_A L_A L_B ... \tag{57}$$

Notice that when we introduce disorder in the inductances of the dual or mixed TL, the generic Equation (3) shows that the disorder appears simultaneously in the diagonal and non-diagonal part.

In dual transmission lines, the localization behavior of the Fibonacci quasi-periodic distribution of inductances L_n, keeping constant the capacitances $C_n = C_0\ \forall n$, has been studied [78] analyzing the spectrum of the generalized Rényi entropies $R_q(\omega)$ versus ω and the spectrum of the inverse participation ratio $N \times IPR(\omega)$ versus ω. For each q value, $R_q(\omega)$ and $N \times IPR(\omega)$ show more than four global sub-bands. This happens because the allowed frequency band of the dual transmission lines is unbounded from above, namely every frequency of the spectrum is greater than a critical frequency ω_c, i.e., $\omega > \omega_c$. At the same time, the spectrum of $R_q(\omega)$ and $N \times IPR(\omega)$ clearly shows the self-replication behavior, where each sub-band is divided into three sub-bands until it is resolvable (see Figures 2 and 3 of Ref. [78]). This localization behavior is characteristic of quasi-periodic Fibonacci systems. Inside each sub-band, we find extended and localized states and gaps. When system size N grows, the number of gaps and localized states increases in such a way that the integrated density of states $IDOS(\omega)$ behaves in a fractal way. As a consequence, the total bandwidth goes to zero in the thermodynamic limit $N \to \infty$. In Figure 3a) we show the Shannon entropy $S(\omega)$ (39), which corresponds to the $R_1(\omega)$ Rényi entropy discussed in Ref. [78]. Notice that the number of global sub-bands is greater than four. Figure 3b) shows the three sub-bands existing in the global sub-band indicated by the vertical arrow in Figure 3a). These previous results about the number of global sub-bands of the dual TL shown in Ref. [78] change when the Fibonacci disorder is introduced in the mixed transmission line [87]. However, the self-replication of the spectrum is maintained for all kinds of mixed TL formed by p direct cells and q dual cells.

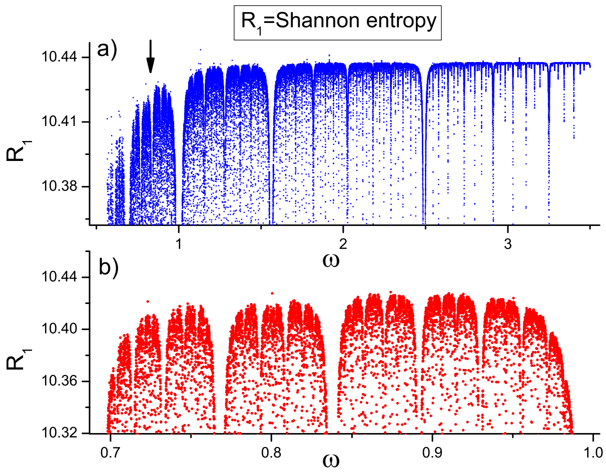

Figure 3. (**a**) Global sub-band structure of the Shannon entropy $S(\omega) = R_1(\omega)$ versus ω, for the Fibonacci quasi-periodic distribution of inductances L_n discussed in Ref. [78]. (**b**) Self-replication structure of the sub-band indicated by the vertical arrow in (**a**).

Remember that mixed TL are generated by a repetition pattern formed by a group of successive p direct cells, followed by a group of successive q dual cells. This topology generates a spectrum of allowed frequencies formed by exactly $d = (p + q)$ bands, as indicated in Section 2.4. In Ref. [87], only the q inductances of the dual cells of mixed TL were distributed according to the Fibonacci sequence, keeping constant the values of the other capacitances and inductances. The localization behavior of the average overlap amplitude (NC_ω) versus ω for the case $p = 2$ and $q = 1$, shows three ($d = 3$) allowed bands (see Figure 10 of Ref. [87]). These d bands exist regardless of the type of disorder and the degree of correlation; however, the position of these d bands depends on the values of all capacitances $(C_{n,x}, C_{n,y})$ and inductances $(L_{n,x}, L_{n,y})$ of direct cells (labeled x) and dual cells (labeled y), and the values of p and q. The average overlap amplitude (NC_ω) versus ω shows four global sub-bands, where each sub-band is divided into three sub-bands until it is resolvable (see Figure 11 of Ref. [87]). This result coincides with the one obtained from the quantum tight-binding model with diagonal Fibonacci disorder. This coincidence occurs because both models (mixed TL and tight-binding model) have bounded spectra and because in both models the Fibonacci disorder appears in the diagonal part of the corresponding dynamic equations (Equations (3) and (5)). Conversely, this result is different from the case of the dual transmission line shown in Figures 2 and 3 of Ref. [78], where the number of global sub-bands is greater than four, because the frequency spectrum of the dual TL is unbounded from the above. Interestingly, when p and q change, each of the $d = (p + q)$ bands of the mixed TL can accommodate a different number of global sub-bands. However, the self-replication is always present. To observe this behavior, let us consider the case with fixed $p = 2$, and two different values of q, namely $q = \{2, 3\}$. Figure 4 shows the average overlap amplitude (NC_ω) versus ω, for (a) $q = 2$ ($d = 4$ bands) and (b) $q = 3$ ($d = 5$ bands). There we can see that the full spectrum of frequencies of mixed TL is contained only within the d bands.

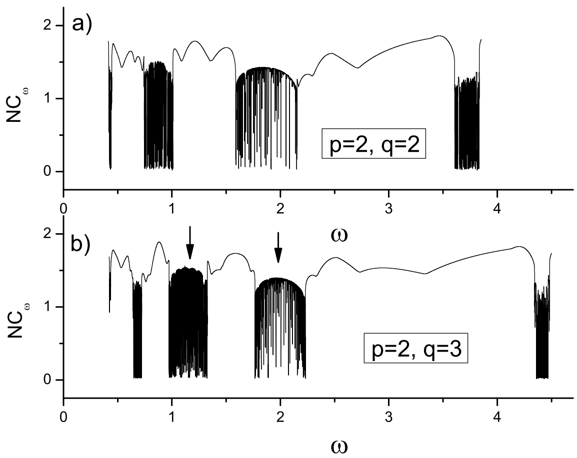

Figure 4. (NC_ω) versus ω for the Fibonacci distribution of inductances L_n, for mixed TL with fixed $p = 2$, considering two values of q. (**a**) $q = 2$ ($d = 4$ bands) and (**b**) $q = 3$ ($d = 5$ bands). Vertical arrows indicate the bands to be studied in Figure 5.

Figure 5 shows (NC_ω) versus ω for the third band and fourth bands shown in Figure 4b. In addition, Figure 5b,d show the self-replication behavior of each sub-band indicated with a vertical arrow in Figure 5a,c, respectively. In this figure we can see that the number of localized states and gaps increases after each self-replication.

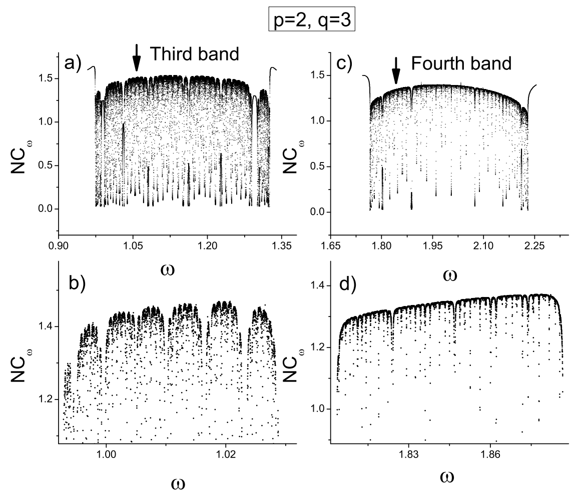

Figure 5. (NC_ω) versus ω for the Fibonacci distribution of inductances L_n for mixed TL, for $p = 2, q = 3$. A detail of Figure 4. (**a**) Third sub-band, (**c**) fourth sub-band. Figures (**b**,**d**) show the self-replication of the sub-bands indicated by vertical arrows in (**a**,**c**), respectively.

In summary, for arbitrary values of p and q forming the mixed TL, the set of $d = (p + q)$ bands accommodates the full spectrum generated by the Fibonacci distribution of inductances L_n. Inside each of the d bands, the number of global sub-bands is always greater than or equal to four, and the self-replication behavior corresponding to quasi-periodic systems is always present. In the self-replication process, new localized states and gaps appear repeatedly. Consequently, the integrated density of states has a fractal behavior and $IDOS\,(\omega) \to 0$ in the thermodynamic limit.

3.1.2. Generalized Thue–Morse Sequence

The generalized Thue–Morse (TM) aperiodic sequence can be generated by means of the substitution rule $A \to A^m B^n$, $B \to B^n A^m$. The corresponding substitution M matrix is given by

$$M = \begin{bmatrix} m & n \\ m & n \end{bmatrix}$$

The λ maximal eigenvalue of M is $\lambda = (m+n)$. For the case $m = 1$ and $n = 1$, we obtain the usual Thue–Morse sequence: $A \to AB$, $B \to BA$, namely

$$A \to AB \to ABBA \to ABBABAAB \to \cdots$$

The maximal eigenvalue $\lambda = (m+n) = 2$ is thus the length of the substitution, which means that $N = \lambda^k$ is the number of the A and B letters in the kth iteration. For the generalized Thue–Morse sequence, the relative frequency of both types of letters, n_A and n_B, is the following $n_A = \frac{m}{(m+n)}$ and $n_B = \frac{n}{(m+n)}$. Another generalization of the Thue–Morse sequence is the $m-$tupling sequence generated by the substitution rule $A \to AB^{m-1}$, $B \to BA^{m-1}$, with $m \geq 2$. In this case, the maximal eigenvalue of the corresponding substitution M matrix is $\lambda = m$, and the number of letters N in this sequence also increases geometrically, i.e., $N = m^k$, where k is the iteration order. Here $n_A = n_B = \frac{1}{2}$. For $m = 2$ we return to the usual Thue–Morse sequence. A spectral classification of one-dimensional binary aperiodic crystals as a function of the substitution matrix M is shown in Ref. [73].

For the tight-binding quantum model, the aperiodic properties of the generalized Thue–Morse systems have been studied in great detail by [47–58,60,62,71]. Additionally, in classical dual and direct transmission lines the Thue–Morse and the $m-$tupling distribution of capacitances and inductances have been studied by [83–85]. For direct TL, two values of inductances L_A and L_B, where distributed according to the $m-$tupling substitution rule $L_A \to L_A L_B^{m-1}$, $L_B \to L_B L_A^{m-1}$, $m \geq 2$, keeping constant the capacitances [83,84]. For $m = 2$ we obtain the usual Thue–Morse substitution rule $L_A \to L_A L_B$, $L_B \to L_B L_A$. One of the principal findings of these studies was that the localization properties of the usual Thue–Morse case, namely $m = 2$, is markedly different to the $m = 3$ case. In general, although in the $m-$tupling sequence the number of letters A and B in each iteration is the same ($n_A = n_B$) for any value of m, the number of extended states in the $m-$tupling inductance distribution depends on the specific value of m. This was demonstrated numerically using different localization tools, like normalized localization length $\Lambda\,(\omega)$, participation number $D\,(\omega)$, normalized participation number $\xi\,(\omega)$, global density of states $DOS\,(\omega)$, transmission coefficient $T\,(\omega)$ and the average overlap amplitude (NC_ω). In addition, it was shown that inside the $m-$tupling family, starting with $m = 3$, the number of extended states increases as the value of m increases, so that for $m >> 3$, the allowed spectrum is similar to the spectrum of the case $m = 2$ (Thue–Morse). This can be seen in Figure 6 where we show the normalized participation number $\xi\,(\omega)$ for three values of m, namely $m = \{2, 3, 13\}$ (a) to (c). Also, in Figure 6d we indicate with a short vertical bar the spectrum of the extended states, namely the frequencies for which the $\Lambda\,(\omega)$ normalized localization length meets the condition $\Lambda\,(\omega) \geq 1$. The image shows that the number of extended states for $m = 3$ is small compared to the case $m = 2$. However, for the case $m >> 3$, namely $m = 8$ and $m = 13$, the number of extended states becomes comparable with case $m = 2$.

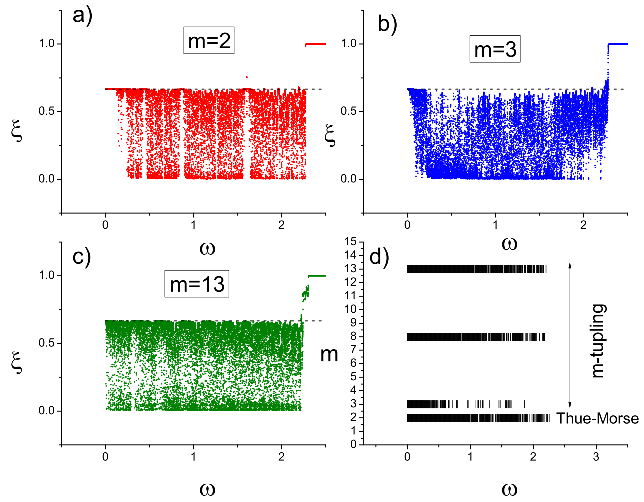

Figure 6. $\xi(\omega)$ versus ω for the $m-$tupling distribution of inductances L_n in the direct TL, for three values of m, namely $m = \{2, 3, 13\}$ (**a**–**c**). (**d**) $\Lambda(\omega)$ versus ω. A short vertical bar indicates the existence of an extended state ($\Lambda(\omega) \geq 1$). The number of extended states for $m = 3$ is very small compared to the case $m = 2$. Conversely, for $m >> 3$ ($m = 8$ and $m = 13$), the number of extended states increases and becomes comparable to the $m = 2$ case.

When comparing the spectrum for cases $m = 2$ and $m = 13$, in a restricted region of frequencies (see Figure 7), it can be observed that the number of extended states which fulfills the condition $\xi \approx 0.667$, corresponding to the periodic case, is reasonably similar in both cases. Also, we can see that the sub-band of extended states of the Thue–Morse case with $m = 2$ (Figure 7a) is much wider than the sub-bands of extended states of the $m-$tupling case with $m = 13$ (Figure 7b).

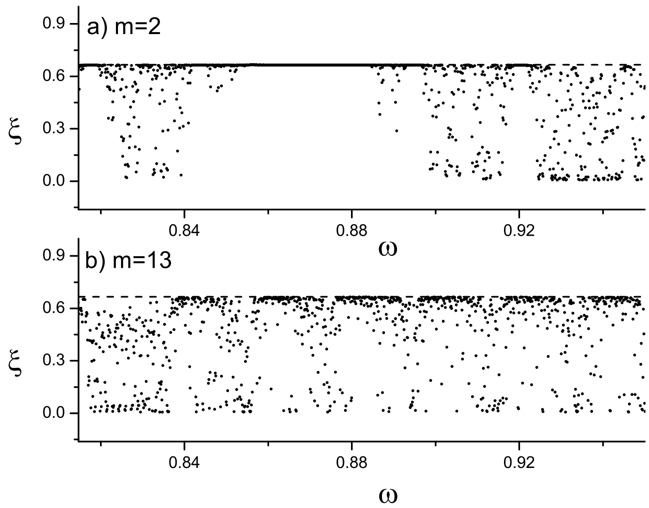

Figure 7. $\xi(\omega)$ versus ω for $m-$tupling distribution of inductances L_n in direct TL in a restricted region of frequencies of the Figure 6. (**a**) $m = 2$, (**b**) $m = 13$. We can see that the sub-bands of extended states ($\xi \approx 0.667$) for $m = 2$ is much wider than the sub-bands of extended states of case $m = 13$.

In sum, for direct transmission lines with $m-$tupling distribution of inductances, the frequency spectrum of the Thue–Morse sequence ($m = 2$) can be considered the limit of the $m-$tupling sequence's frequency spectrum when $m \gg 3$. On the other hand, the number of extended states for the case $m = 2$ decreases dramatically when m changes to $m = 3$, as shown in Refs. [83,84] and Figure 6.

As an extension of these ideas, the localization behavior of dual transmission lines with non-linear capacitances has been studied [85]. The non-linear behavior of capacitances is introduced through the $V_{C,n}$ potential difference across each capacitance, i.e.,

$$V_{C,n} = q_n \left(\frac{1}{C_n} - \varepsilon_n \left| q_n \right|^2 \right) \tag{58}$$

C_n is the linear part of the capacitance $V_{C,n}$ and ε_n is the amplitude of the non-linear term. The equation corresponding to this dual case is given by

$$\left(L_{n-1} + L_n - \frac{1}{\omega^2 C_n} + \frac{\varepsilon_n \left| I_n \right|^2}{\omega^4} \right) I_n - L_{n-1} I_{n-1} - L_n I_{n+1} = 0 \tag{59}$$

When the non-linear amplitudes ε_n go to zero ($\varepsilon_n \to 0$), we return to the dual linear Equation (2). The localization behavior of this non-linear dual TL has been studied using two values of the non-linear amplitude ε_n, namely ε_A and ε_B, distributed according to the $m-$tupling Thue–Morse sequence [85], i.e., $\varepsilon_A \to \varepsilon_A \, \varepsilon_B^{m-1}$, $\varepsilon_B \to \varepsilon_B \, \varepsilon_A^{m-1}$, $m \geq 2$, but keeping constant the capacitances C_n and inductances L_n, namely $C_n = C_0$, and $L_n = L_0 \; \forall n$. In this case, the aperiodic disorder appears only in the diagonal term of the dynamic Equation (59).

The same fundamental result about the localization degree of the $m = 2$ case in comparison with the $m \geq 3$ case reappears in this non-linear case, that is, for fixed values of ε_A and ε_B, the $m \geq 3$ family does not belong to the family corresponding to $m = 2$, and in addition, for $m >> 3$ the frequency spectrum begins to resemble the spectrum of the case $m = 2$. To be specific, for $m = 2$ we can see a large number of extended states across the entire frequency spectrum, mixed with localized states and gaps. On the contrary, for $m = 3$, almost the entire frequency spectrum is formed with localized states and gaps, accordingly showing a huge decrease in the number of extended states. This behavior can be seen in Figure 6 of Ref. [85] that shows $\xi(\omega)$ versus ω for $m = \{2, 3, 5, 9\}$. To compare the cases for $m = 2$ and $m = 3$ in more detail, in Figure 8 we show the average overlap amplitude $\langle NC_\omega \rangle$, for $m = \{2, 3\}$ with $\varepsilon_A = 0.1$ and $\varepsilon_A = 0.03$, keeping constant the values of capacitances C_n and inductances L_n. When m changes from $m = 2$ to $m = 3$, the number of extended states decreases markedly, almost tending to zero. The horizontal dashed line corresponds to the periodic linear case, $\varepsilon_A = \varepsilon_B = 0$, for which $\langle NC_\omega \rangle$ fulfills the condition $\langle NC_\omega \rangle \approx 1.62$. Moreover, at the top of each figure, we indicate with a short vertical bar the presence of an extended state, namely $\Lambda(\omega) \geq 1$. Both results about the number and position of the extended states in each case match each other. This localization behavior coincides with the results shown in Figure 6 of Ref. [85], when studying the localization behavior of the normalized participation number $\xi(\omega)$ and $\Lambda(\omega)$. This way, we have demonstrated that the $m = 2$ (Thue–Morse) case is different than the $m = 3$ case ($m-$tupling).

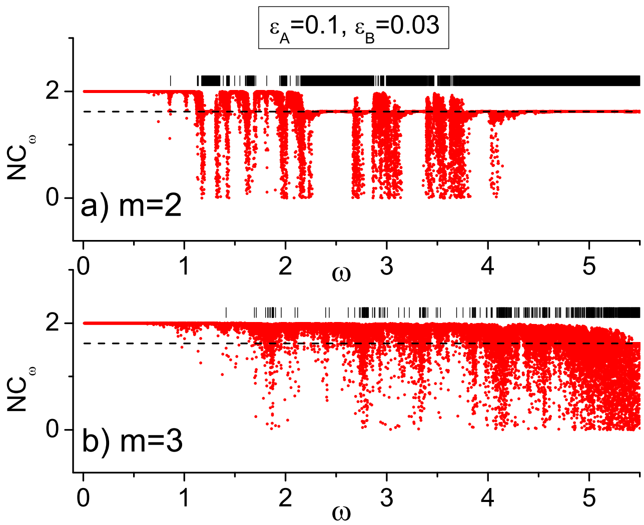

Figure 8. (NC_ω) versus ω for the $m-$tupling distribution of amplitudes ε_n of non-linear capacitances of the dual TL with $\varepsilon_A = 0.1$ and $\varepsilon_B = 0.03$. (**a**) Case $m = 2$ and (**b**) case $m = 3$. The horizontal dashed lines indicate the value $(NC_\omega) \approx 1.62$, for the periodic linear case, i.e., $\varepsilon_A = \varepsilon_B = 0.0$. In addition, at the top of each figure, we indicate with a vertical bar the presence of extended states which meet condition $\Lambda(\omega) \geq 1$.

Consider now the localization behavior of the integrated density of states $IDOS(\omega)$ for the non-linear case, with $\varepsilon_A = 0.1$ and $\varepsilon_A = 0.03$. In Figure 9a we show the $IDOS(\omega)$ for four values of m, namely $m = \{2, 3, 8, 13\}$. For each m we use a constant size $N_m = m^k$, namely $N_m = \{2^{21}, 3^{13}, 8^7, 13^6\}$. There we can see that for the case $m = 2$, the $IDOS(\omega)$ is always greater than the $IDOS(\omega)$ of any other value of $m \geq 3$. However, when m grows ($m = 8$ and $m = 13$), the $IDOS(\omega)$ grows, approaching the values for the case $m = 2$. This behavior confirms the conjecture that the Thue–Morse sequence ($m = 2$) can be considered to be a limit case of the $m-$tupling sequence when $m \gg 3$. We now turn to the behavior of the $IDOS(\omega)$ for fixed $m = 3$, as a function of the $N = 3^k$ system size, with $k = \{10, 12, 13\}$ (see Figure 9b). For the minimum value $k = 10$, the $IDOS(\omega)$ is the greatest of all, but when N increases (the value of k increases), the number of extended states decreases (the $IDOS(\omega)$ decreases), and new localized states and gaps appear that barely contribute to the integrated density of states. As a consequence, the $IDOS(\omega)$ tends to zero. This behavior is characteristic of aperiodic systems.

On the other hand, for fixed value of m, when the difference $|\varepsilon_A - \varepsilon_B|$ between the values of the amplitudes of the non-linear term increases, so does the disorder degree of the transmission line, which tends to localize the electric current function $I(\omega)$, and as a result, the integrated density of states $IDOS(\omega)$ go to zero. This behavior can be observed in Figure 5 of Ref. [85], for $m = 2$ (Thue–Morse case), considering a fixed value $\varepsilon_A = 0.0$ (the periodic linear case) and three different values of ε_B, namely $\varepsilon_B = \{0.01, 0.03, 0.07\}$.

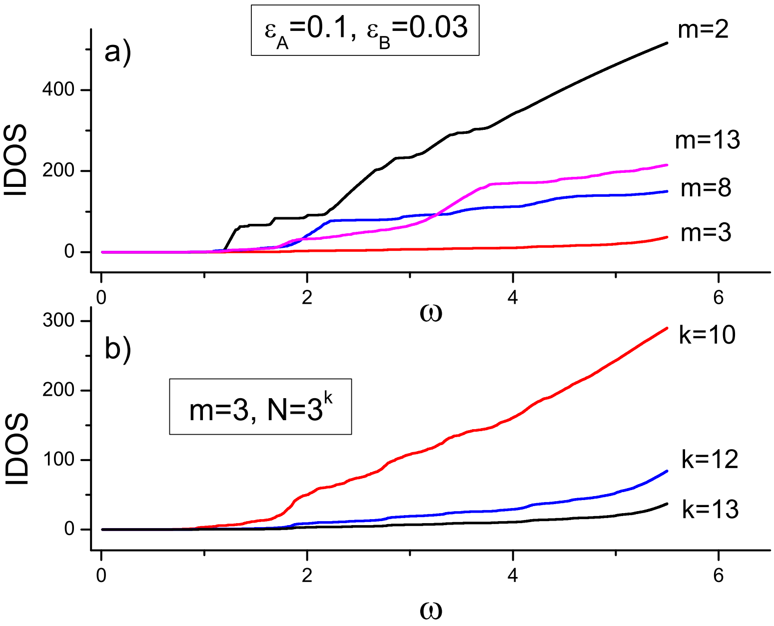

Figure 9. The integrated density of states $IDOS\,(\omega)$ versus ω for the $m-$tupling distribution of amplitudes ε_n of the non-linear capacitances of the dual TL for $\varepsilon_A = 0.1$ and $\varepsilon_B = 0.03$. (**a**) $IDOS$ for four m values, i.e., $m = \{2, 3, 8, 13\}$. For each m, we used a fixed N_m, i.e., $N_m = \left\{2^{21}, 3^{13}, 8^7, 13^6\right\}$. The $IDOS$ for $m = 2$ is the greatest of all, and the $IDOS$ for $m = 3$ is the smallest of all. For increasing values of m ($m = 8$ y $m = 13$), the $IDOS$ tends to the value corresponding to $m = 2$. (**b**) Fixed $m = 3$, as a function of the $N = m^k$, with $k = \{10, 12, 13\}$. The $IDOS$ corresponding to $N = 3^{10}$ is the largest of all. When N increases, the $IDOS$ tends to zero, $IDOS \to 0$.

3.1.3. Incommensurate Sequences

The aperiodic incommensurate systems are generated by two superimposed periodic structures with incommensurate periods. The origin of incommensurability may be structural or dynamic. In the first case, two or more superimposed periodic structures with incommensurate periods exist, and in the second case one periodicity is related to the crystalline structure and the other to the behavior of elementary excitations that propagate through the crystal. Two of the most studied incommensurate models are the Aubry–André model and the Soukoulis–Economou model.

In the one-dimensional tight-binding quantum model, the site energies ε_n have been distributed according to the Aubry–André model that is

$$\varepsilon_n = \varepsilon_0 + b\cos\left(2\pi\beta n\right) \tag{60}$$

where ε_0 is the single-site energy of the unperturbed periodic lattice, b is the amplitude and β is an irrational number, usually $\beta = 0.5\left(\sqrt{5} - 1\right)$ (the inverse of the Fibonacci golden mean). For $b = 2.0$, a phase transition from extended to localized states appears [36,69,70,72].

In classical electric transmission lines, the Aubry–André model has been used to distribute the inductances L_n in two different cases: (a) direct TL with constant capacitances $C_n = C_0\ \forall n$ (diagonal disorder) [86] and (b) mixed transmission lines with disorder only in the q inductances of the dual cells, keeping constant the value of all the other electrical components of the direct and dual cells [87]. In this case, the disorder appears in the diagonal and the off-diagonal terms of the generic Equation (3).

In case a), the inductances L_n of the direct transmission line are distributed according to the Aubry–André sequence:

$$L_n = L_0 + b\cos(2\pi\beta n) \tag{61a}$$

where $L_0 = const.$ and $b < L_0$. In this case, the aperiodic incommensurate disorder only appears in the diagonal term of the generic Equation (3). The localization behavior of this classic electric model can be visualized in Figure 10 where the map (b,ω) is shown for $L_0 = 4.0$ and $N = 7 \times 10^5$. Each dot on the map indicates the existence of an extended state, because the normalized localization length fulfills condition $\Lambda(\omega) \geq 1.0$. For $b \to 0$, the frequency spectrum shows a single band of extended states that corresponds to the periodic case. For increasing values of b, i.e., for $b \leq 1.9$, the map (b,ω) shows three global sub-bands of extended states (with localized states and gaps) separated by two large gaps. After that, for $b > 1.9$, only two global sub-bands of extended states survive, which also contain localized states and gaps. Finally, for b close to $b = L_0$, there is only a small sub-band where almost all states are extended states, namely $0 \leq \omega \leq 0.45$.

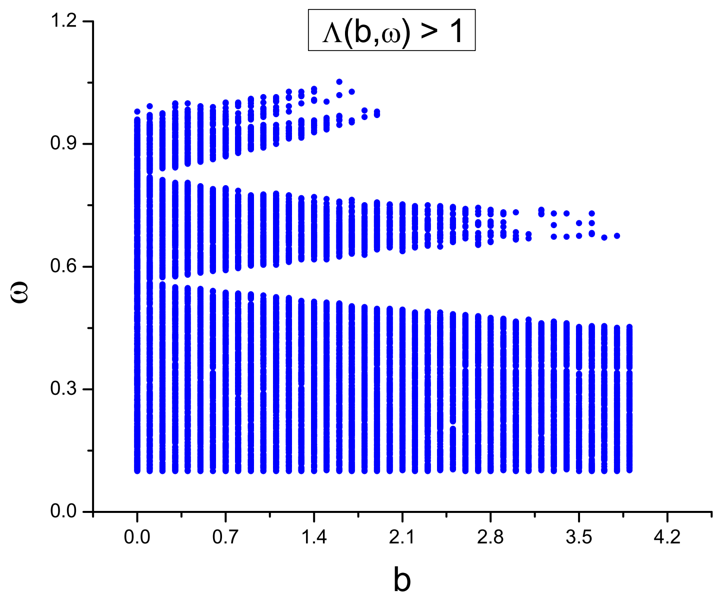

Figure 10. Map (b,ω) for the Aubry–André distribution of inductances with $L_0 = 4.0$. Each point of the map indicates an extended state, because $\Lambda(\omega) \geq 1.0$. For increasing values of the amplitude b, the number of sub-bands of extended states diminishes, and for b close to $b = L_0$, there is only a small sub-band where almost all states are extended states, namely $0 \leq \omega \leq 0.45$.

Figure 11 shows (a) the $\lambda(\omega)$ Lyapunov exponent versus ω for two values of the b amplitude $b = \{1.5, 3.99\}$ and b the spectrum of the extended states, $\Lambda(\omega) \geq 1$ versus ω for fixed $b = 1.5$. Figure 11a shows that for $b = 3.99 \approx L_0$ (thick red line), only one band of extended states ($\lambda(\omega) \to 0$) can be observed for $\omega \leq 0.45$. Conversely, for $\omega > 0.45$, only gaps and localized states can be found for this value of b. This result coincides with the result indicated by the map shown in Figure 10. On the other hand, in the same Figure 11a we draw $\lambda(\omega)$ versus ω for a smaller value of b, namely $b = 1.5$ (thin black line). There we can see several sub-bands of extended states ($\lambda(\omega) \to 0$) separated by gaps. Within these sub-bands, we can find more localized states and gaps, which are not perceived in this picture. On the contrary, these gaps can be seen in Figure 11b, where a detail of the map Figure 10 is shown for $b = 1.5$, for fixed $N = 10^6$. In this figure, each short vertical bar indicates an extended state, because $\Lambda(\omega) \geq 1.0$. The vertical dashed arrows that cross both figures (for the case $b = 1.5$) indicate the edge of the gaps, i.e., the frequencies for which phase transitions occur.

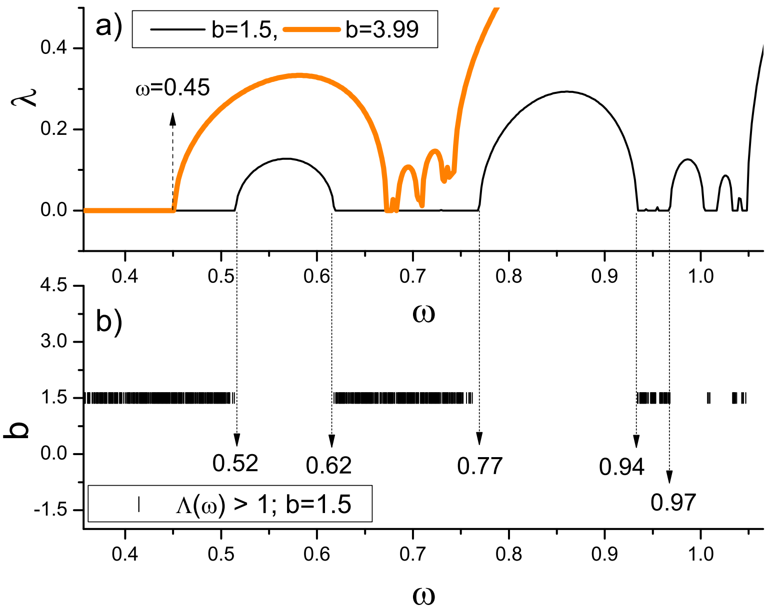

Figure 11. (**a**) Lyapunov exponent $\lambda(\omega)$ versus ω for two values of the b amplitude $b = \{1.5, 3.99\}$. For $b = 3.99 \approx L_0$ (thick red line), only one band of extended states ($\lambda(\omega) \to 0$) can be observed for $\omega \leq 0.45$. Conversely, for $b = 1.5$ (thin black line), we can see several sub-bands of extended states ($\lambda(\omega) \to 0$) separated by gaps. Within these sub-bands, we can find more localized states and gaps. (**b**) The spectrum of the extended states, $\Lambda(\omega) \geq 1$ versus ω for fixed $b = 1.5$ and $N = 10^6$. The vertical dashed arrows that cross both images indicate the edge of the gaps, in which phase transitions occur.

To see in more detail the phase transition from extended to localized states, in Figure 12a we show the Lyapunov exponent $\lambda(\omega)$ versus ω for the cases $b = 2.0$ and $N = 2 \times 10^5$. The vertical arrows indicate the frequencies $\omega_1 = 0.5006231$, $\omega_2 = 0.6336884$, and $\omega_3 = 0.7577136$, to be studied in Figure 12b–d, respectively. In these last three images, we show the scaling behavior of the average overlap amplitude (NC_ω) for three values of N, namely $N = \{8, 12, 16\} \times 10^4$. For each frequency ω_1, ω_2 and ω_3, we find a phase transition from extended states to localized states at the critical value $b_c = 2.0$. To the left of the critical point b_c for almost every amplitude b, all (NC_ω) values coalesce into a single one, i.e., $(NC_\omega) \to const > 0$, indicating an extended behavior. On the contrary, to the right of the critical point ($b > b_c$), (NC_ω) grows as system size N grows, indicating a localized behavior.

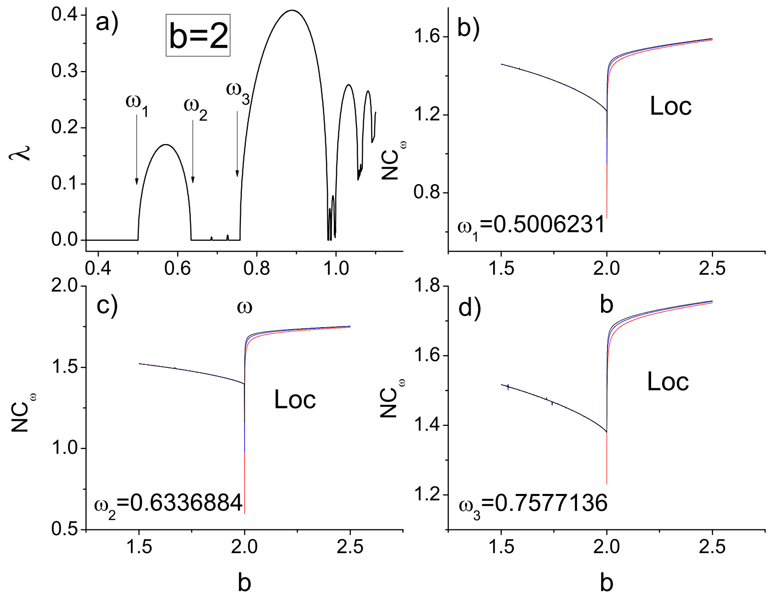

Figure 12. (**a**) Lyapunov exponent $\lambda\,(\omega)$ versus ω for the case $b = 2.0$ and $N = 2 \times 10^5$. The vertical arrows indicate the frequencies $\omega_1 = 0.5006231$, $\omega_2 = 0.6336884$, and $\omega_3 = 0.7577136$, to be studied in (**b**–**d**). In these last three images, we show the scaling behavior of (NC_ω) for three values of N, namely $N = \{8, 12, 16\} \times 10^4$. For each frequency ω_1, ω_2 and ω_3, we can see a phase transition from extended states to localized states at the critical value $b_c = 2.0$. For $b \leq b_c$ we find only extended states, because for almost every amplitude b, all (NC_ω) values coalesce into a single one, i.e., $(NC_\omega) \to const. > 0$. On the contrary, for $b > b_c$, (NC_ω) grows as system size N grows, indicating a localized behavior.

These results coincide with those in Figures 4–6 of Ref. [86], where this same problem was studied. In [86], a phase transition from the extended to the localized state is found depending on amplitude parameter b. This result was found for different frequency values, by studying transmission coefficient $T\,(\omega)$ and the scaling behavior of the average overlap amplitude (NC_ω).

In case (b), for mixed transmission lines (with p direct cells and q dual cells), the inductances L_n of the q dual cells were distributed according to the Aubry–André sequence [87], namely $L_{n,y} = L_{0,y} + b \cos\cos\,(2\pi\beta n)$ with $b < L_{0,y}$. All other electric components are kept constant, i.e., for direct cells $L_{n,x} = L_{0,x}$, $C_{n,x} = C_{0,x}$ and for dual cells $C_{n,y} = C_{0,y}$. In Ref. [87], three different cases were studied: (a) $p = 2, q = 1$, (b) $p = 1, q = 4$ and (c) $p = 4, q = 1$. In all cases, the frequency spectrum is completely contained within the $d = (p + q)$ bands generated by the mixed TL. For fixed b, in each of the d bands, it is always possible to find sub-bands of extended states in addition to localized states and gaps. These results were obtained by studying the transmission coefficient $T\,(\omega)$ and the scaling of the average overlap amplitude (NC_ω) (see Figures 7–9 of Ref. [87]). To see the influence of the b amplitude in the localization behavior, in Figure 13 we show the transmission coefficient $T\,(\omega)$ for four values of b, namely $b = \{0.3, 0.7, 1.1, 1.5\}$ for the case $p = 2$, $q = 1$. We use the same values of the electric components used in Ref. [87]. In particular, $L_{0,y} = 1.6$. For $b = 0.3$ we find $d = 3$ bands containing extended states, localized states and gaps (similar to Figure 7a of Ref. [87]). However, for increasing values of b, the number of extended states within each band decreases, and as a consequence both lateral bands begin to disappear. In this way, for $b = 1.1$, the leftmost band has already disappeared, and for $b = 1.5$, the rightmost band is about to disappear.

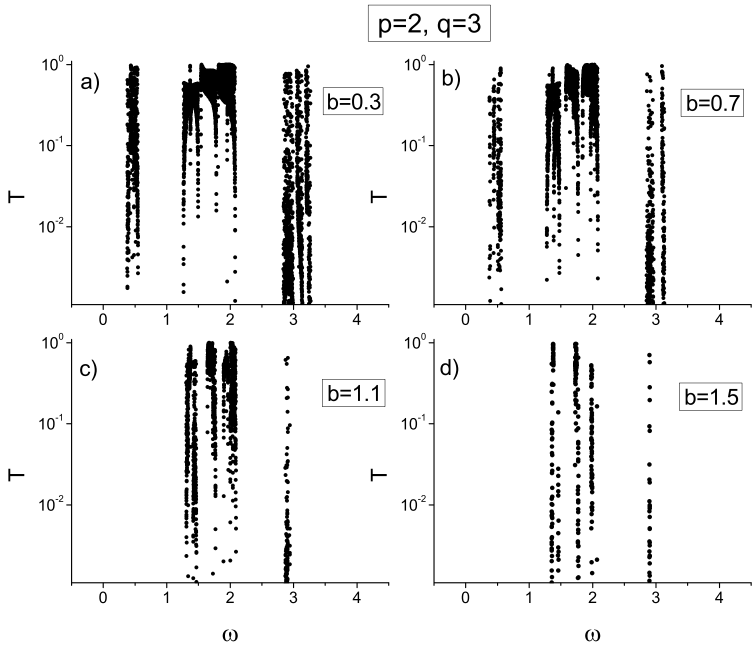

Figure 13. Transmission coefficient $T(\omega)$ versus ω, for mixed transmission line with $p = 2$, $q = 1$, for (**a**) $b = 0.3$, (**b**) $b = 0.7$, (**c**) $b = 1.1$ and (**d**) $b = 1.5$. For (**a**) $b = 0.3$ we find $d = (p+q) = 3$ bands containing extended states, localized states and gaps. For increasing values of b, the number of extended states within each band decreases. Therefore, for (**c**) $b = 1.1$, the leftmost band has already disappeared, and for (**d**) $b = 1.5$, the rightmost band is about to disappear.

3.2. Long-Range Correlated Disorder

For one-dimensional disordered systems without any correlation in the disorder (white noise), all states are localized states in the thermodynamic limit. However, the introduction of correlation in the disorder can trigger the appearance of a discrete set of extended states (short-range correlation) or bands of extended states (long-range correlation). The correlated disorder has been introduced in quantum tight-binding systems [2–29] and in classical systems such as harmonic chains [96–99], and electrical transmission lines [76,77,79,80,88].

The quantum tight-binding Equation (5) and the generic Equation (3) describing transmission lines are similar. Transformations (6) and (7) permit the correspondence between both models. However, unlike the quantum case, in transmission lines it is impossible to study the pure off-diagonal case, because the disorder contained in the vertical impedances (the coupling between neighboring electric cells) appears in the off-diagonal coefficients B_{n-1} and B_n of the generic Equation (3) and in the diagonal coefficient $D_n = (B_{n-1} + B_n - A_n)$ too.

To analyze the main differences in the localization behavior with the one-dimensional quantum case, the dual, direct and mixed disordered transmission lines have been studied recently. These studies include long-range correlated disorder and diluted disordered TL. In addition to continuous sequences, the long-range correlation has been used to generate discrete sequences (binary and ternary).

3.2.1. Discrete Sequences

To generate long-range correlated sequences $\{x_n\}$ we use the Fourier filtering method (FFM). Let us consider initially a set of uncorrelated random numbers $\{u_n\}$ with a Gaussian distribution. Then we take the fast Fourier transform (FFT) of the random sequence $\{u_n\}$ and we obtain a new sequence $\{u_k\}$. The long-range correlation is introduced in the sequence $\{u_k\}$ doing the following transformation $x_k = u_k k^{-\frac{1}{2}(2\alpha-1)}$. Calculating the inverse FFT of the new sequence $\{x_k\}$, we obtain the long-range correlated sequence $\{x_n\}$ which is spatially correlated with the $S(k)$ spectral density

$S(k) \propto k^{-(2\alpha-1)}$. Here the exponent α of the transformation is known as the correlation exponent and fulfills the condition $\alpha \geq 0.5$. For $\alpha = 0.5$, we regain the uncorrelated random sequence (white noise). Correlation exponent α quantifies the degree of long-range correlation imposed in the original random sequence $\{u_n\}$. Finally, we normalize the correlated sequence $\{x_n\}$ to obtain zero average, $\langle x_n \rangle = 0$, and the variance is set to unity.

From the long-range correlated sequence $\{x_n(\alpha > 0.5)\}$, we can generate the asymmetric ternary sequence $\{v_n(b_1, b_2)\}$ formed with three letters, A, B and C,

$$v_n = \begin{cases} A & \text{if } x_n < b_1 \\ C & \text{if } b_1 \leq x_n \leq b_2 \\ B & \text{if } x_n > b_2 \end{cases} \tag{62}$$

with $b_2 \geq b_1$. The symmetric ternary map is obtained when $b_2 = -b_1 = b$. If $b_1 = b_2 = b$ we obtain the asymmetric binary sequence $\{A, B\}$. For $b \to 0$ we regain the symmetric binary sequence. Please note that the long-range correlation of the ternary sequence $\{v_n(b_1, b_2)\}$ is not exactly quantified by the correlation exponent α, because the map (62) changes the long-range correlation. In one-dimensional tight-binding systems, the symmetric binary and ternary model has been studied [8,24,25,28]. In these models, a metal-insulator transition has been reported as a function of the correlation degree α and size b of the window. In addition, the asymmetric ternary map (62) was studied using electrical dual transmission lines [76] considering three values of capacitances $C_n = \{C_A, C_B, C_C\}$, maintaining constant the inductances $L_n = L_0\ \forall n$. This case contains only diagonal disorder. The long-range correlation in the distribution of capacitances was generated through the FFM. For TL with a finite number of cells, it is possible to find bands of extended states whose size increases for increasing values of correlation exponent α. For the asymmetrical model, the normalized localization length $\Lambda(\omega, \alpha, b_1, b_2, N)$ is a complicated function of the parameters ω, α, b_1, b_2, and N, but for fixed frequency ω, for $N \to \infty$, it is always possible to find a transition from localized electric current functions to extended current functions for some specific values of the parameters. For the symmetrical ternary map $b_2 = -b_1 = b$, a phase diagram (α, b) separating localized states from extended states has been found for fixed frequency performing finite-size scaling of the normalized localization length $\Lambda(\omega)$. This result is similar to the phase diagram found in the tight-binding case.

Moreover, the same ternary dual TL was studied, but using the Ornstein–Uhlenbeck method to generate the long-range correlation [77]. In this method, the degree of long-range correlation depends on two independent parameters, i.e., the viscosity coefficient γ and the diffusion coefficient C. Studying the scaling behavior of $\Lambda(\omega)$, we obtain two-phase diagrams for the symmetrical map when C and γ are independent parameters, namely (C, b) for fixed γ and (γ, b) for fixed C. In addition, we study the phase diagrams when C and γ are dependent parameters, i.e., $C = \gamma^2$. In all cases, we find a transition from localized to extended states. Also, the harmonic symmetric ternary chain was studied in Ref. [99] using the Ornstein–Uhlenbeck method for the case $C = \gamma^2$. Instead of the transition from localized to extended behavior, they found a disorder-order transition for $b > 4$, because the disorder degree practically disappears at this limit.

This same kind of disorder-order transition has been found by studying localization properties of direct TL with diluted and non-diluted asymmetric dichotomous noise (binary sequences of inductances L_A and L_B with $C_n = C_0\ \forall n$) [82]. The asymmetric dichotomous sequence $\{\zeta(t)\}$ is generated by a variable $\zeta(t)$ which switches in time in a random way between two given values a and $(-b)$ with transition rates μ_a and μ_b, respectively (dichotomous noise). Considering $\zeta(t)$ as a stationary process, the dichotomous noise has zero mean and is exponentially correlated. The τ correlation time of the dichotomous noise is defined as $\tau^{-1} = (\mu_a + \mu_b)$. In addition, from the zero-average condition $\langle \zeta(t) \rangle = 0$, we obtain the following relationship between a, b, μ_a and μ_b, namely $\beta = \frac{a}{b} = \frac{\mu_a}{\mu_b}$, where parameter β measures the degree of asymmetry of the dichotomous noise. For $\mu_a > \mu_b$ we have $\beta > 1$ and for $\mu_a < \mu_b$ we have $\beta < 1$. The symmetric sequence $\mu_a = \mu_b$ is obtained for the case $\beta = 1$. Consequently, the dichotomous noise is characterized by three independent parameters: τ,

a and b. However, setting the value of one of the parameters, for example, $b = 1$, we can study the localization behavior generated by this kind of exponentially correlated noise using only two independent parameters, i.e., τ and β. In the diagonal disordered direct TL, the inductances L_A and L_B are distributed according to the asymmetric dichotomous noise, keeping the capacitances constant $C_n = C_0 \; \forall n$ [82]. For $\tau < \tau_c$ and for $\beta < \beta_c$ (τ_c, β_c are critical values) the electric current function $I(\omega)$ shows a localized behavior, but for $\tau > \tau_c$ and for $\beta > \beta_c$, the $D(\omega, \tau, \beta)$ participation number scales as $D(\omega) \propto N^{m(\omega,\tau,\beta)}$, where $m(\omega, \tau, \beta) < 1$ is the slope of the linear relationship between $\ln(D(\omega, \tau, \beta))$ and $\ln(N)$, for fixed ω, β, and τ. Only in the limit $\tau \to \infty$ (for fixed ω and β) and $\beta \to \infty$ (for fixed ω and τ), we obtain the exact linear behavior, i.e., $\lim_{\tau\to\infty} m(\omega, \tau, \beta) = 1.0$ and $\lim_{\beta\to\infty} m(\omega, \tau, \beta) = 1.0$. However, in both limits, $\tau \to \infty$ or $\beta \to \infty$, the asymmetric dichotomous sequence becomes a periodic sequence. Thus, we only can observe a disorder-order transition, which in turn indicates that all states are localized states in the thermodynamic limit for classical electric TL. This result coincides with the one obtained for the one-dimensional tight-binding quantum model with symmetric dichotomous noise, in which the metal-insulator transition is absent [56,100].

3.2.2. Continuous Sequences

In addition to discrete sequences, continuous long-range correlated sequences have been used to study the localization behavior of direct, dual and even mixed electrical transmission lines [79,80,88]. In general, in classical electric transmission lines, the long-range correlated disorder in capacitances and inductances has been used in the following form:$C_n(\alpha) = C_0 + b\, f(x_n(\alpha))$ and $L_n(\beta) = L_0 + b\, f(y_n(\beta))$, where $f(u)$ is an harmonic function. $\{x_n(\alpha)\}$ and $\{y_n(\beta)\}$ are two independent long-range correlated sequences generated by the FFM and α and β are the corresponding correlation exponents that determine the correlation degree. b is the amplitude of the fluctuation of C_n and L_n around C_0 and L_0, respectively. The diagonal and off-diagonal disordered dual transmission line, considering only one type of correlated sequence $\{x_n(\alpha)\}$ has been studied recently [79]. In this case, C_n and L_n vary in phase, i.e.,

$$\begin{aligned} C_n &= C_0 + b \sin(2\pi x_n(\alpha)) \\ L_n &= L_0 + b \sin(2\pi x_n(\alpha)) \end{aligned} \tag{63}$$

Here, $b < \min(C_0, L_0)$ to avoid negative values of the electrical components. For this kind of disorder, it is always possible to find extended states for different frequencies, and for each specific frequency a phase diagram (b, α), which separates extended states from localized states in the thermodynamic limit can be found.

To obtain the critical correlation exponent α_c separating localized states from extended states, we analyze the scaling behavior of (a) the participation number $D(\omega)$ (37), (b) the relative fluctuation $\eta_D(\omega, b, \alpha, N)$ of the participation number $D(\omega)$ and (c) the Binder cumulant $B_D(\omega, b, \alpha, N)$ of the participation number $D(\omega)$. These quantities are defined as

$$\eta_D(\omega, b, \alpha, N) = \sqrt{\left(\frac{\langle D^2\rangle}{\langle D\rangle^2} - 1\right)} \tag{64}$$

and

$$B_D(\omega, b, \alpha, N) = \left(1 - \frac{\langle D^4\rangle}{3\langle D^2\rangle^2}\right) \tag{65}$$

where $\langle .. \rangle$ means an average over long-range correlated sequences.

For increasing system size N, the relative fluctuation η_D goes to zero for extended states and grows converging to a finite value for localized states. Consequently, for $N \to \infty$, η_D tends toward a step function and a discontinuity appears that separates extended states from localized states. This scaling behavior can be used to determine the critical correlation exponent α_c for fixed values of ω

and b, because the curves $\eta_D(\alpha)$ with different N values will cross in a single point (the critical point α_c). Also, the scaling behavior of the Binder cumulant $B_D(\alpha)$ indicates that for $N \to \infty$, $B_D(\alpha)$ jumps abruptly from a constant value ($B_D = 0.667$) for extended states to zero ($B_D(\alpha) = 0$) for localized states. Consequently, for fixed values of ω and b, the curves $B_D(\alpha)$ with different N values will cross in a single point (critical point α_c). On the other hand, the critical value of the fluctuation amplitude b_c can be obtained studying the scaling behavior of the normalized localization length $\Lambda(b)$ (35). For fixed ω and $\alpha \geq \alpha_c$, in the transition point from localized to extended states, $\Lambda(b)$ varies from $\Lambda(b) > 1$ to $\Lambda(b) \to 0$. Finally, in the thermodynamic limit, for fixed frequency ω, the phase diagram (b, α) is formed by two independent straight lines, so that extended states only appear when condition $\alpha \geq \alpha_c$ is met for any $b \leq b_c$. Specifically, in Ref. [79] the following values were used: $C_0 = 0.5$, $L_0 = 1.0$. For the fixed frequency $\omega = 3.6$, the critical values are $b_c = 0.43$ and $\alpha_c = 1.51$ (see phase diagram in Figure 9 of Ref. [79]). In Figure 14 we show, in a schematic way, the phase diagram for a fixed frequency ω, when C_n and L_n vary in phase (63) in dual TL. This map is conceptually different to the map in Figure 15b), when C_n and L_n vary out of phase (in the study of mixed TL).

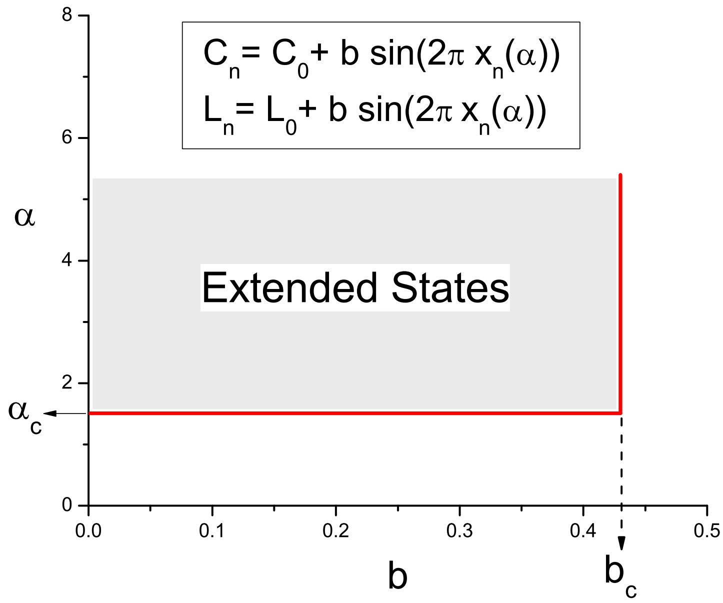

Figure 14. Schematic phase diagram (b, α), for a fixed frequency ω, when C_n and L_n vary in phase in dual transmission lines. For this transmission line with long-range correlated distribution of C_n and L_n, extended states can only be found for $\alpha \geq \alpha_c$ and $b \leq b_c$.

In Ref. [88], this model was generalized in two ways: (a) studying mixed transmission lines instead of dual TL, and (b) the capacitances $C_{n,y}$ and inductances $L_{n,y}$ of the dual cells of mixed TL are distributed out of phase, using two independent long-range correlated sequences $x_n(\alpha) \neq y_n(\beta)$. Specifically,

$$\begin{aligned} C_{n,y} &= C_{0,y} + b\cos(2\pi x_n(\alpha)) \\ L_{n,y} &= L_{0,y} + b\cos(2\pi y_n(\beta)) \end{aligned} \tag{66}$$

where $\{x_n(\alpha)\}$ and $\{y_n(\beta)\}$ are two independent long-range correlated sequences, even in the case $\alpha = \beta$, because each correlated sequence is initiated using two independent uncorrelated random sequences according to the FFM. The localization behavior of this mixed TL was studied in Ref. [88] for the case $p = 2$, $q = 3$. The frequency spectrum of this case shows $d = (p + q) = 5$ bands. Additionally, in the thermodynamic limit, for fixed p, q and b, it is always possible to find an asymmetric phase diagram (α, β) for each frequency ω, corresponding to an extended state. In the case studied in Ref. [88], for $\omega = 1.986591$ and $b = 0.1$, the correlation exponents α and β fulfill the following condition: $\alpha \geq \alpha_c$ and $\beta \geq \beta_c$, with the asymmetric condition $\alpha_c \geq \beta_c$. This behavior can be observed in Figures 8 and 9 of Ref. [88]. There we can see the phase diagram (α, β) that separates localized states from extended states, and the localization behavior of $\Lambda(\omega)$ versus α (for fixed β), and $\Lambda(\omega)$ versus β (for fixed α). The asymmetric condition $\alpha_c \geq \beta_c$ can be explained through the following arguments. In relationships (66), the fluctuation $\Delta C_{n,y}$ of the capacitances around $C_{0,y}$ is the same as the fluctuation of inductances $\Delta L_{n,y}$ around $L_{0,y}$, namely $\Delta C_{n,y} = \Delta L_{n,y} = 2b$. However, in every kind of transmission line, capacitances only appear in the form $C_{n,y}^{-1}$. Accordingly, the fluctuation of this term is given by $\Delta C_{n,y}^{-1} = \left(\frac{2b}{g}\right)$, where $g = \left(C_{0,y}^2 - b^2\right)$. For $g < 1$ we have $\Delta C_{n,y}^{-1} > \Delta L_{n,y}$, which means that the term $C_{n,y}^{-1}$ introduces a greater disorder into the generic Equation (3) than the disorder introduced by $L_{n,y}$. This fact can induce a decrease in the degree of correlation of the sequence $\{C_n(\alpha)\}$. To compensate this decrease, correlation exponent α must be greater than correlation exponent β of $L_{n,y}(\beta)$ to generate extended states. Consequently, the critical correlation exponents fulfill the condition $\alpha_c \geq \beta_c$, as long as condition $\left(C_{0,y}^2 - b^2\right) < 1$ is valid. Also, for fixed ω, and for given correlation exponents α and β, it is possible to find a critical value of amplitude b of the fluctuation, in such a way that for $b \geq b_c$ all states are localized states (see Figures 10 and 11 of Ref. [88]).

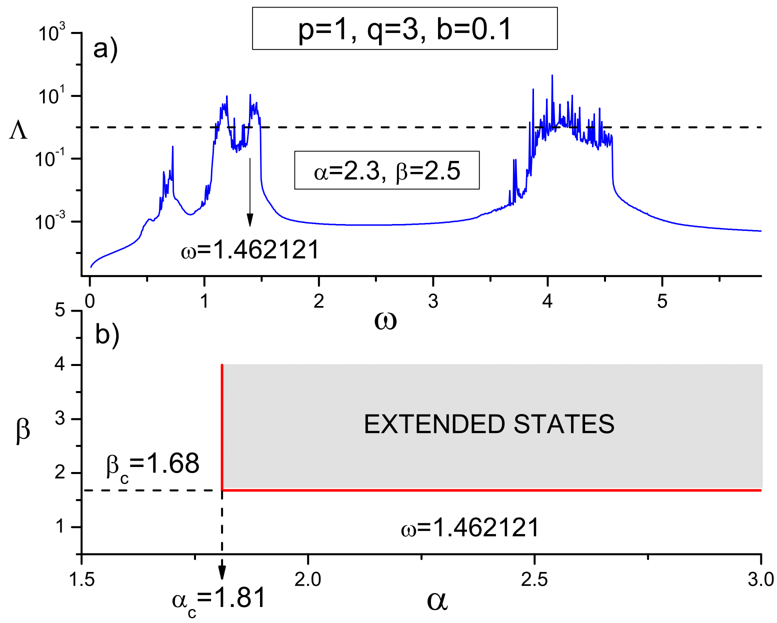

Figure 15. (**a**) $\Lambda(\omega)$ versus ω, for mixed TL with $p = 1$ and $q = 3$, for $b = 0.1$. We consider two fixed values of the correlation exponents, $\alpha = 2.3$ and $\beta = 2.5$. Only three bands are visible, because $\Lambda(\omega) \to 0$ for the leftmost band (localized states). (**b**) Phase diagram (α, β) for $\omega = 1.462121$ (indicated by the vertical arrow in (**a**)). Only for $\alpha \geq \alpha_c = 1.81$ and $\beta \geq \beta_c = 1.68$, with $\alpha_c > \beta_c$ is it possible to find extended states.

The localization behavior of mixed transmission lines with long-range correlated disorder given by (66) can be summarized in Figures 15 and 16, where we studied mixed TL with $p = 1$ and $q = 3$. This case has $d = 4$ bands. Figure 15a shows $\Lambda(\omega)$ versus ω for $b = 0.1$, for two fixed values of the correlation exponents, namely $\alpha = 2.3$ and $\beta = 2.5$. Only three bands are visible, because $\Lambda(\omega) \to 0$ for the leftmost band (localized states). The vertical arrow indicates the specific frequency $\omega = 1.462121$ studied in Figures 15b and 16. For this frequency, Figure 15b shows the phase diagram (α, β). This image indicates that only for $\alpha \geq \alpha_c$ and $\beta \geq \beta_c$, with $\alpha_c > \beta_c$ it is possible to find extended states.

Also, for $\omega = 1.462121$, the critical correlation exponents are $\alpha_c = 1.81$ and $\beta_c = 1.68$. Please note that the asymmetric condition $\alpha_c > \beta_c$ is fulfilled. Figure 16 shows the scaling behavior of the average overlap amplitude $\ln(C_\omega)$ versus $\ln(N)$ for the frequency $\omega = 1.462121$ indicated by vertical arrows in Figure 15a. For fixed $\beta = 3.6$ we obtain the critical value α_c of the correlation exponent, namely $\alpha_c = 1.81$ (see Figure 16a). For $\alpha < \alpha_c$ all states are localized states because we cannot obtain a linear relationship between $\ln(C_\omega)$ and $\ln(N)$. However, for $\alpha \geq \alpha_c$ we only find straight lines with the same slope $m = -1.0$ ($R = 1.0$). This behavior indicates that (NC_ω) is constant for increasing values of N. This is exactly the scaling behavior of the average overlap amplitude for extended states. For fixed $\alpha = 2.0$, Figure 16b shows the same kind of scaling behavior, obtaining $\beta_c = 1.68$.

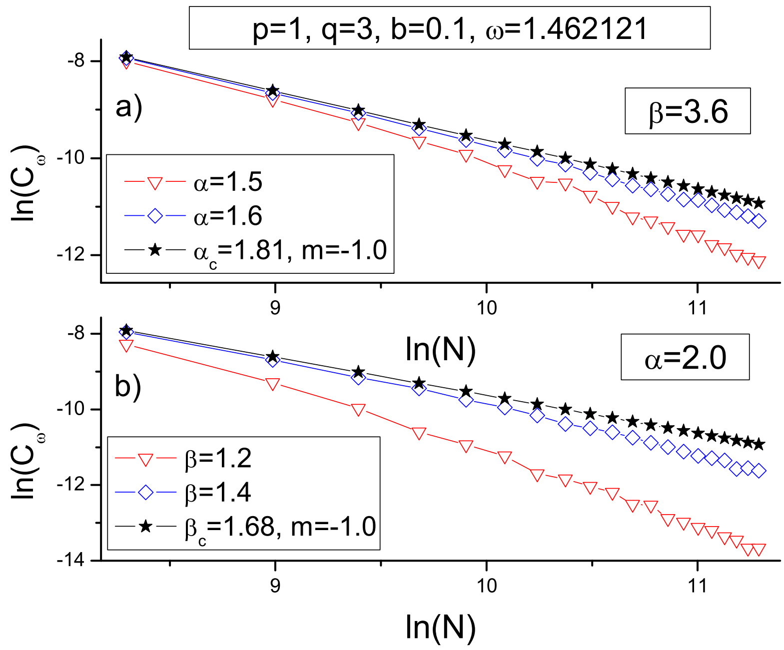

Figure 16. Scaling behavior of $\ln(C_\omega)$ versus $\ln(N)$ for mixed TL with $p = 1$, $q = 3$, $\omega = 1.462121$, and $b = 0.1$. (**a**) For fixed $\beta = 3.6$, only for $\alpha \geq \alpha_c = 1.81$, we find straight lines with the same slope $m = -1.0$ ($R = 1.0$), which indicates an extended behavior. (**b**) For fixed $\alpha = 2.0$, only for $\beta \geq \beta_c = 1.68$, we can obtain linear relationships with $m = -1.0$.

3.3. Diluted Disordered Systems

Hilke [101] introduced the diluted Anderson model, which considers two interpenetrating lattices, i.e., a pure lattice ($\varepsilon_j = \varepsilon_0$), while an Anderson lattice (ε_{jP} is a random number) is periodically distributed with period $P \geq 1$. This means $(P-1)$ diluting elements exist between two Anderson sites. For $P = 1$ we regain the usual Anderson model [1]. This model was generalized [11,12] so that the $(P-1)$ diluting elements are distributed according to a function with certain specific symmetry conditions (see Ref. [11]). The case $\varepsilon_j = \varepsilon_0$ is the most symmetrical of all, and coincides with the results from previous works [101–103]. Depending on the type of symmetry, the dilution process can generate a maximum of up to $(P-1)$ extended states, which are exactly located on some of the edges of the gaps. For constant off-diagonal term, the position of these resonances depends only on the period P and the values of ε_j of the diluting elements. At the same time, resonances are independent of the type of disorder, as well as the degree of correlation in the disordered lattice. In addition, in the resonance, the extended wave function behaves like an intermediate extended function, because its amplitude is zero at each disordered site. The localization behavior of the diluted systems have been studied in the tight-binding quantum case, and in classic systems, like harmonic chains and electric transmission lines [11,12,15,23,80–82,84,96,101–103].

Let us consider the localization behavior of diluted direct transmission lines, with constant capacitances, i.e., $C_n = C_0 \; \forall n$. The inductances L_n, corresponding to disordered sites, have been distributed in different forms. Between two disordered inductances, L_n and L_{n+P}, we put $(P-1)$ identical inductances $L_0 = const.$, where $L_n \neq L_0$. Consequently, the inductances are distributed in the following schematic way ... L_x L_0 L_0 L_0 L_x L_0 L_0 L_0 L_x ..., where $P = 4$. Because of the full symmetry of the diluting elements, we find exactly $(P-1)$ resonances and $(P-1)$ gaps [11]. For direct transmission lines, resonance frequencies are obtained analytically [80–82]:

$$\begin{aligned} P &= 2, \quad \omega = \sqrt{2}\omega_0 \\ P &= 3, \quad \omega = \sqrt{2 \pm 1}\omega_0 \\ P &= 4, \quad \omega = \left\{ \sqrt{2}, \sqrt{2 \pm \sqrt{2}} \right\} \omega_0 \end{aligned} \tag{67}$$

where $\omega_0 = (L_0 C_0)^{-\frac{1}{2}}$ and $L_0 \neq L_n$.

In Ref. [80] the inductances L_n were distributed in (a) a random way, and (b) considering long-range correlated disorder (Fourier Filtering method and Ornstein–Uhlenbeck process). In both cases a continuous distribution of L_n values was used. In addition, in Ref. [81] the inductances L_n were distributed by means of an aperiodic binary sequence of Galois [67], and in Ref. [82] the inductances L_n were distributed considering an asymmetric dichotomous sequence. In all cases studied, the existence of $(P-1)$ intermediate extended states has been demonstrated. Also, the position of the resonance frequencies coincides with theoretical predictions.

On the other hand, the localization behavior of the diluted aperiodic $m-$tupling distribution of inductances was studied in Ref. [84]. The case $m = 3$ was considered, with $(P-1) = 4$ diluting elements L_0. For numerical calculation, the following data were used: $C_n = C_0 = 0.5 \; \forall n$, $L_A = 1.6$, $L_B = 1.5$ and $L_0 = 1.8$. Figure 6 of Ref. [84] shows (a) the overlap amplitude (NC_ω), and (b) the normalized participation number $\xi(\omega)$. In that picture we can see four gaps and four resonances, which are indicated by vertical dashed lines. Notice that resonances are placed at the left edge of each gap. This result coincides with the theoretical predictions. In Figure 17, we show the average overlap amplitude (NC_ω) for the same case studied in Figure 6 of Ref. [84], but now we study the Thue–Morse sequence, i.e., $m = 2$. Here, we consider four values of P, namely $P = \{1, 2, 3, 4\}$. The case $P = 1$ corresponds to the usual Thue–Morse sequence without dilution. According to (67), for each $P \geq 2$, the frequency of the resonances are: $P = 2$, $\omega = \{1.491\}$; $P = 3$, $\omega = \{1.054, 1.826\}$, and $P = 4$, $\omega = \{0.807, 1.491, 1.948\}$. These theoretical values coincide with the numerical results shown in Figure 17. The same localization behavior of this diluted aperiodic system can be seen in Figure 18 studying the density of states $DOS(\omega)$ versus ω. There we can see that to the left of each gap, the density of states does not fluctuate, which is an indication of the extended nature of the resonance located there. This does not happen on the right side of each gap.

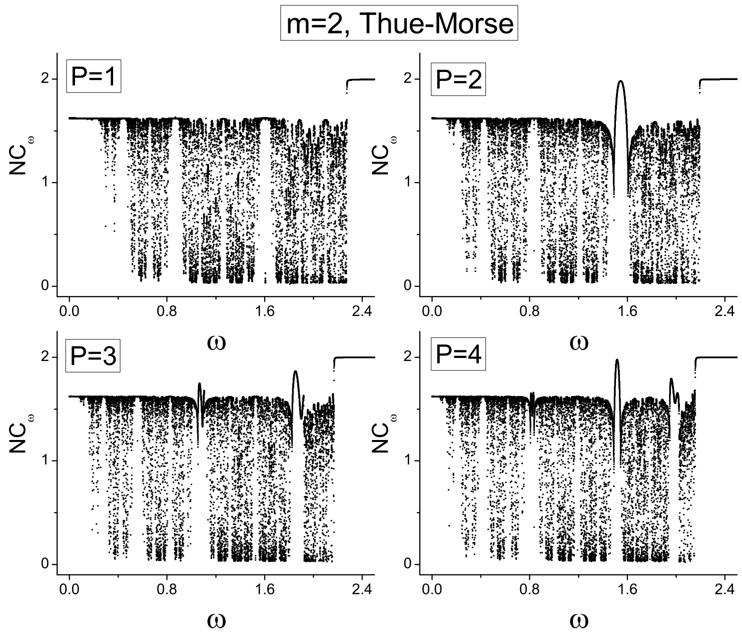

Figure 17. (NC_ω) versus ω, for the Thue–Morse distribution of inductances, with $L_A = 1.6$, $L_B = 1.5$. Four values of the period P are considered, namely $P = \{1, 2, 3, 4\}$. The case $P = 1$ corresponds to the usual Thue–Morse sequence without dilution. For $P \geq 2$, the sequences are diluted with $L_0 = 1.8$, with fixed $C_n = 0.5$. The resonances coincide with the left edge of each of the $(P - 1)$ gaps generated by the dilution process.

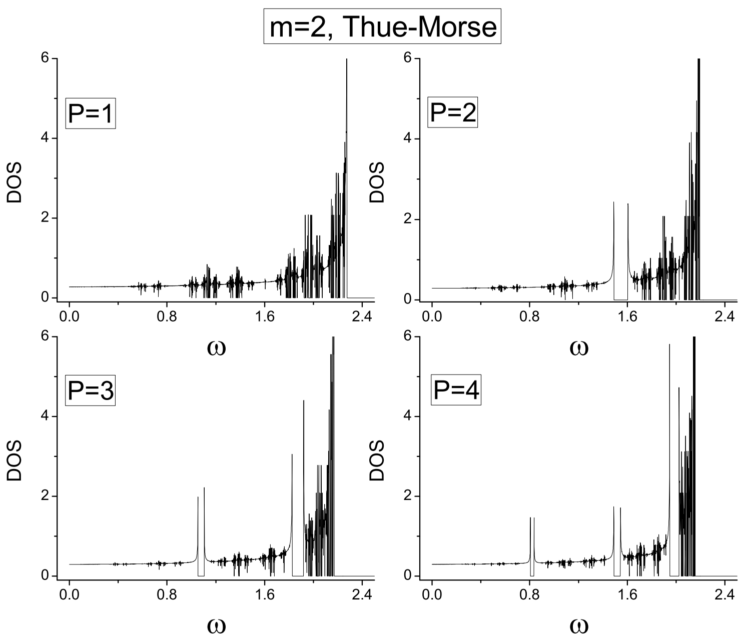

Figure 18. Density of states $DOS\ (\omega)$ versus ω. To the left of each gap, the density of states does not fluctuate, which is an indication of the extended nature of the resonance located there. The same does not happen on the right side of each gap. In addition, we can see that the localization behavior of the $DOS\ (\omega)$, is identical to the localization behavior shown by (NC_ω) in Figure 17.

4. Summary and Conclusions

We have presented the results of the study of the localization properties of disordered electrical transmission lines. This study considered three types of TL: dual, direct and mixed. The electrical components of the (capacitances and inductances) were distributed in different non-periodic forms: (a) aperiodic, which included self-similar sequences (Fibonacci and $m-$tupling Thue–Morse), (b) incommensurate sequences (Aubry–André and Soukoulis–Economou), and (c) long-range correlated sequences (binary discrete and continuous). The localization properties of these classical systems were measured using the typical tools used in quantum mechanics to characterize the localization behavior of disordered systems. Specifically, we used the normalized localization length $\Lambda(\omega)$, the inverse participation ratio $IPR(\omega)$, the transmission coefficient $T(\omega)$, the global density of states $DOS(\omega)$, the average overlap amplitude C_ω, and others. Our studies indicate that the localization behavior of classic electric transmission lines is quite similar to the one-dimensional tight-binding quantum model, but at the same time it is possible to observe some significant differences; therefore, it is worth continuing to investigate this type of classical disordered systems.

As a possible application of the study of the localization properties of disordered electric transmission lines, we can consider the neuronal axons that connect two or more neurons through electrical impulses. The axon, which usually is covered by a myelin sheath, can be considered to be a transmission line formed by Schwann cells connected by nodes of Ranvier. It has been established that there exist certain specific genes responsible for stabilizing the internal neuronal structure, which in turn allows the proper transport of the electrical impulse within the axon. The electrical communication between neurons fails if axons are damaged or broken. This can happen in the earliest stages of neurodegenerative diseases or for other reasons. Based on the localization properties of electrical transmission lines studied in this review, it is possible to conclude that electrical communication between neurons prevails, if Schwann cells and Ranvier nodes are distributed in a periodic way or in a very specific aperiodic way. On the contrary, any non-correlated disorder in the axon structure will stop the electrical impulses and the neurons will remain without communication. Consequently, to restore electrical communication between neurons, I can conjecture that the genes responsible for stabilizing the internal neuronal structure have the specific mission of restoring periodicity in the distribution of Schwann cells and Ranvier's nodes.

Up to that point, we have only considered ideal transmission lines, i.e., transmission lines without dissipation (resistance $R = 0$). When we introduced gain ($R_n = -R$, n odd) and loss ($R_n = +R$, n even) balanced pairwise, a $\mathcal{PT}$-symmetric resistive configuration is obtained. For this dissipative system, we can find a critical resistance R_c such that for $R < R_c$ the frequency spectrum is completely real, but for $R > R_c$ the frequency spectrum contains real and complex frequencies. This phenomenon is called a $\mathcal{PT}$-symmetric transition phase, because the TL goes from an unbroken ($R < R_c$) to a broken $\mathcal{PT}$-symmetric phase as a function of resistance R. In addition, we have demonstrated that in the unbroken $\mathcal{PT}$-symmetric phase, the electric current function $I_n(\omega)$ is a symmetric extended function. Conversely, in the broken phase, $I_n(\omega)$ is an antisymmetric localized function. This phase transition was recently found for TL with a very small number of cells considering fixed boundary conditions [89].

In addition to this research, we are currently studying two different lines of research, (a) the influence of non-linear inductances or capacitances in the stability and amplitude of the allowed conducting bands of the unbroken $\mathcal{PT}$-symmetric phase, and (b) the localization behavior of some models of structured transmission lines, in the spirit of the structured systems proposed by Chakrabarti [29]. Specifically, we analyzed TL with a finite number of hanging cells (direct or dual) in random positions in TL. The electric components (capacitances or inductances) of each hanging cell, can contain aperiodic disorder or long-range correlated disorder.

Funding: This research was funded by Dirección de Investigación, Postgrado y Transferencia Tecnológica de la Universidad de Tarapacá, Arica, Chile, grant number 4737-19.

Acknowledgments: The author is grateful for the collaboration of my colleagues and my students who, during the last decade, helped me in the study of the localization properties of disordered electrical transmission lines.

Conflicts of Interest: The author declares no conflict of interest.

Abbreviations

The following abbreviations are used in this manuscript:

TL	Transmission Lines
FFM	Fourier Filtering Method
FFT	Fast Fourier Transform

References

1. Anderson, P.W. Absence of diffusion in certain random lattices. *Phys. Rev.* **1958**, *109*, 1492. [CrossRef]
2. Mott, N.F.; Twose, W.D. The theory of impurity conduction. *Adv. Phys.* **1961**, *10*, 107. [CrossRef]
3. Thouless, D.J. Electrons in disordered systems and the theory of localization. *Phys. Rep.* **1974**, *13*, 93. [CrossRef]
4. Flores, J.C. Transport in models with correlated diagonal and off-diagonal disorder. *J. Phys. Condens. Matter* **1989**, *1*, 8471. [CrossRef]
5. Lifshits, I.M.; Gredeskul, S.A.; Pastur, L.A. *Introduction to the Theory of Disordered Systems*; Wiley: New York, NY, USA, 1989.
6. Dunlap, D.H.; Hu, H.-L.; Philips, P.W. Absence of localization in a random-dimer model. *Phys. Rev. Lett.* **1990**, *65*, 88. [CrossRef]
7. Philips, P.W.; Hu, H.-L. Localization and its absence: A new metallic state for conducting polymers. *Science* **1991**, *252*, 1805. [CrossRef] [PubMed]
8. de Moura, F.A.B.F.; Lyra, M.L. Delocalization in the 1D Anderson model with long-range correlated disorder. *Phys. Rev. Lett.* **1998**, *81*, 3735. [CrossRef]
9. Izrailev, F.M.; Krokhin, A.A. Localization and the mobility edge in one-dimensional potentials with correlated disorder. *Phys. Rev. Lett.* **1999**, *82*, 4062. [CrossRef]
10. Izrailev, F.M.; Krokhin, A.A.; Ulloa, S.E. Mobility edge in aperiodic Kronig-Penney potentials with correlated disorder: Perturbative approach. *Phys. Rev. B* **2001**, *63*, 041102(R). [CrossRef]
11. Lazo, E.; Onell, M.E. Extended states in 1-D Anderson chain diluted by periodic disorder. *Physica B* **2001**, *299*, 173. [CrossRef]
12. Lazo, E.; Onell, M.E. Existence of the delocalized states in two interpenetrated 1-D diluted Anderson chains. *Phys. Lett. A* **2001**, *283*, 376. [CrossRef]
13. Carpena, P.; Galvan, P.B.; Ivanov, P.C.; Stanley, H.E. Metal-insulator transition in chains with correlated disorder. *Nature* **2002**, *418*, 955. [CrossRef] [PubMed]
14. Deych, L.I.; Erementchouk, M.V.; Lisyanky, A.A. Scaling properties of the one-dimensional Anderson model with correlated diagonal disorder. *Phys. Rev. B* **2003**, *67*, 024205. [CrossRef]
15. de Moura, F.A.B.F.; Santos, M.N.B.; Fulco, U.L.; Lyra, M.; Lazo, E.; Onell, M.E. Delocalization and wave-packet dynamics in one-dimensional diluted Anderson models. *Eur. Phys. J. B* **2003**, *36*, 81. [CrossRef]
16. Zhang, W.; Ulloa, S.E. Extended states in disordered systems: role of off-diagonal correlations. *Phys. Rev. B* **2004**, *69*, 153203. [CrossRef]
17. Shima, H.; Nomura, T.; Nakayama, T. Localization-delocalization transition in one-dimensional electron systems with long-range correlated disorder. *Phys. Rev. B* **2004**, *70*, 075116. [CrossRef]
18. Titov, M.; Schomerus, H. Nonuniversality of Anderson localization in short-range correlated disorder. *Phys. Rev. Lett.* **2005**, *95*, 126602. [CrossRef] [PubMed]
19. Izrailev, F.M.; Makarov, N.M. Anomalous transport in low-dimensional systems with correlated disorder. *J. Phys. A* **2005**, *38*, 10613. [CrossRef]
20. Shima, H.; Nakayama, T. Breakdown of Anderson localization in disordered quantum chains. *Microelectr. J.* **2005**, *36*, 422. [CrossRef]

21. de Moura, F.A.B.F.; Malyshev, A.V.; Lyra, M.L.; Malyshev, V.A.; Domínguez-Adame, F. Localization properties of a one-dimensional tight-binding model with nonrandom long-range intersite interactions. *Phys. Rev. B* **2005**, *71*, 174203. [CrossRef]
22. Díaz, E.; Rodriguez, A.; Domínguez-Adame, F.; Malyshev, V.A. Anomalous optical absorption in a random system with scale-free disorder. *Europhys. Lett.* **2005**, *72*, 1018. [CrossRef]
23. Albuquerque, S.S.; de Moura, F.A.B.F.; Lyra, M.L.; Lazo, E. Sensitivity to initial conditions of the wave-packet dynamics in diluted Anderson chains. *Phys. Lett. A* **2006**, *355*, 468. [CrossRef]
24. Esmailpour, A.; Esmaeilzadeh, M.; Faizabadi, E.; Carpena, P.; Reza Rahimi Tabar, M. Metal-insulator transition in random Kronig-Penney superlattices with long-range correlated disorder. *Phys. Rev. B* **2006**, *74*, 024206. [CrossRef]
25. Esmailpour, A.; Cheraghchi, H.; Carpena, P.; Reza Rahimi Tabar, M. Metal–insulator transition in a ternary model with long range correlated disorder. *J. Stat. Mech.* **2007**, P09014. [CrossRef]
26. Kaya, T. Localization-delocalization transition in chains with long-range correlated disorder. *Eur. Phys. J. B* **2007**, *55*, 49. [CrossRef]
27. Benhenni, R.; Senouci, K.; Zekri, N.; Bouamrane, R. Anderson transition in 1D systems with spatial disorder. *Physica A* **2010**, *389*, 1002. [CrossRef]
28. Izrailev, F.M.; Krokhin, A.A.; Makarov, N.M. Anomalous localization in low-dimensional systems with correlated disorder. *Phys. Rep.* **2012**, *512*, 125. [CrossRef]
29. Chakrabarti, A. Electronic states and charge transport in a class of low dimensional structured systems. *Phys. E Low-Dimen. Syst. Nanostruct.* **2019**, *114*, 113616. [CrossRef]
30. Bellani, V.; Diez, E.; Hey, R.; Toni, L.; Tarricone, L.; Parravicini, G.B.; Dominguez-Adame, F.; Gómez-Alcalá, R. Experimental evidence of delocalized states in random dimer superlattices. *Phys. Rev. Lett.* **1999**, *82*, 2159. [CrossRef]
31. Kulh, U.; Izrailev, F.M.; Krokhin, A.A.; Stöckmann, H.-J. Experimental observation of the mobility edge in a waveguide with correlated disorder. *Appl. Phys. Lett.* **2000**, *77*, 633.
32. Krokhin, A.A.; Izrailev, F.M.; Kulh, U.; Stöckmann, H.-J.; Ulloa, S.E. Random 1D structures as filters for electrical and optical signals. *Physica E* **2002**, *13*, 695. [CrossRef]
33. Kulh, U.; Izrailev, F.M.; Krokhin, A.A. Enhancement of localization in lne-dimensional random potentials with long-range correlations. *Phys. Rev. Lett.* **2008**, *100*, 126402.
34. Lugan, P.; Aspect, A.; Sanchez-Palencia, L.; Delande, D.; Grémaud, B.; Muller, C.A.; Miniatura, C. One-dimensional Anderson localization in certain correlated random potentials. *Phys. Rev. A* **2009**, *80*, 023605. [CrossRef]
35. Dietz, O.; Kulh, U.; Stöckmann, H.-J.; Makarov, N.M.; Izrailev, F. Microwave realization of quasi-one-dimensional systems with correlated disorder. *Phys. Rev. B* **2011**, *83*, 134203. [CrossRef]
36. Aubry, S.; André, G. Analyticity breaking and Anderson localization in incommensurate lattices. *Ann. Isr. Phys. Soc.* **1980**, 3, 133.
37. Kohmoto, M.; Kadanoff, L.P.; Tang, C. Localization Problem in One Dimension: Mapping and Escape. *Phys. Rev. Lett.* **1983**, *50*, 1870. [CrossRef]
38. Ostlund, S.; Pandit, R.; Rand, D.; Schellnhuber, H.J.; Siggia, E.D. One-dimensional Schrödinger equation with an almost periodic potential. *Phys. Rev. Lett.* **1983**, *50*, 1873. [CrossRef]
39. Sokoloff, J.B. Unusual band structure, wave functions and electrical conductance in crystals with incommensurate periodic potentials. *Phys. Rep.* **1985**, *126*, 189. [CrossRef]
40. Kohmoto, M.; Banavar, J.R. Quasiperiodic lattice: Electronic properties, phonon properties, and diffusion. *Phys. Rev. B* **1986**, *34*, 563. [CrossRef]
41. Kohmoto, M. Localization problem and mapping of one-dimensional wave equations in random and quasiperiodic media. *Phys. Rev. B* **1986**, *34*, 5043. [CrossRef]
42. Nori, F.; Rodríguez, J.P. Acoustic and electronic properties of one-dimensional quasicrystals. *Phys. Rev. B* **1986**, *34*, 2207. [CrossRef] [PubMed]
43. Niu, Q.; Nori, F. Renormalization-group study of one-dimensional quasiperiodic systems. *Phys. Rev. Lett.* **1986**, *57*, 2057. [CrossRef] [PubMed]
44. Lu, J.P.; Odagaki, T.; Birman, J.L. Properties of one-dimensional quasilattices. *Phys. Rev. B* **1986**, *33*, 4809. [CrossRef] [PubMed]

45. Fujita, M.; Machita, K. Electrons on one-dimensional quasi-lattices. *Solid State Commun.* **1986**, *59*, 61. [CrossRef]
46. Liu, Y.; Riklund, R. Electronic properties of perfect and nonperfect one-dimensional quasicrystals. *Phys. Rev. B* **1987**, *35*, 6034. [CrossRef] [PubMed]
47. Zaks, M.A.; Pikovsky, A.S.; Kurths, J. On the correlation dimension of the spectral measure for the Thue-Morse sequence. *J. Stat. Phys.* **1987**, *88*, 1387. [CrossRef]
48. Riklund, R.; Severin, M.; Liu, Y. The Thue-Morse aperiodic crystal, a link between the Fibonacci quasicrystal and the periodic crystal. *Int. J. Mod. Phys. B* **1987**, *1*, 121. [CrossRef]
49. Cheng, Z.; Savit, R.; Merlin, R. Structure and electronic properties of Thue-Morse lattices. *Phys. Rev. B* **1988**, *37*, 4375. [CrossRef]
50. Luck, J.M. Cantor spectra and scaling of gap widths in deterministic aperiodic systems. *Phys. Rev. B* **1989**, *39*, 5834. [CrossRef]
51. Kolář, M.; Ali, M.; Nori, F. Generalized Thue-Morse chains and their physical properties. *Phys. Rev. B* **1991**, *43*, 1034. [CrossRef]
52. Ryu, C.S.; Oh, G.Y.; Lee, M.H. Extended and critical wave functions in a Thue-Morse chain. *Phys. Rev. B* **1992**, *46*, 5162. [CrossRef] [PubMed]
53. Huang, D.; Gumbs, G.; Kolar, M. Localization in a one-dimensional Thue-Morse chain. *Phys. Rev. B* **1992**, *46*, 11479. [CrossRef] [PubMed]
54. Ryu, C.S.; Oh, G.Y.; Lee, M.H. Electronic properties of a tight-binding and a Kronig-Penney model of the Thue-Morse chain. *Phys. Rev. B* **1993**, *48*, 132. [CrossRef] [PubMed]
55. Chakrabarti, A.; Karmakar, S.N.; Moitra, R.K. Role of a new type of correlated disorder in extended electronic states in the Thue-Morse lattice. *Phys. Rev. Lett.* **1995**, *74*, 1403. [CrossRef] [PubMed]
56. Deych, L.I.; Zaslavsky, D.; Lisyansky, A.A. Wave localization in generalized Thue-Morse superlattices with disorder. *Phys. Rev. E* **1997**, *56*, 4780. [CrossRef]
57. Oh, G.Y. Existence of Extended Eletronic States in the Thue-Morse Lattice. *J. Korean Phys. Soc.* **1997**, *31*, 808.
58. Oh, G.Y. Quantum dynamics of an electron in a one-dimensional Thue-Morse Lattice. *J. Korean Phys. Soc.* **1998**, *33*, 617.
59. Lazo, E.; Onell, M.E. Localization in one-dimensional systems with generalized Fibonacci disorder. *Revista Mexicana de Física* **1998**, *44*, 52.
60. Maciá, E.; Domínguez-Adame, F. *Electrons, Phonons and Excitons in Low Dimensional Systems*; Editoral Complutense S. A.: Madrid, Spain, 2000.
61. Hui-Fen, G.; Rui-Bao, T. Extended state to localization in random aperiodic chains. *Commun. Theor. Phys.* **2006**, *46*, 929. [CrossRef]
62. Min, N.; Zhixlong, W. A property of m-tuplings morse sequence. *Wuhan Univ. Nat. Sci.* **2006**, *11*, 473. [CrossRef]
63. Maciá, E. The role of periodic order in science and technology. *Rep. Prog. Phys.* **2006**, *22*, 397 [CrossRef]
64. Janssen, T.; Chapuis, G.; de Boissieu, M. *Aperiodic Crystals: From Modulated Phases to Quasicrystals*; Oxford University Press: Oxford, UK, 2007.
65. Steurer, W.; Deloudi, S. *Cristallography of Quasicrystals—Concept, Methods and Structures*; Springer Series in Material Science 126; Springer: Berlin, Germany, 2009.
66. Maciá, E. *Aperiodic Structures in Condensed Matter*; CRC Taylor and Francis: Boca Raton, FL, USA, 2009.
67. Wan, R.; Fu, X. Localization properties of electronic states of one-dimensional Galois sequences. *Solid State Commun.* **2010**, *150*, 919. [CrossRef]
68. Maciá, E. Exploiting aperiodic designs in nanophotonic devices. *Rep. Prog. Phys.* **2012**, *75*, 036502. [CrossRef] [PubMed]
69. Cheng, W.W.; Gong, L.Y.; Shan, C.J.; Sheng, Y.B.; Zhao, S.M. Geometric discord characterize localization transition in the one-dimensional systems. *Eur. Phys. J. D* **2013**, *67*, 121. [CrossRef]
70. Cheng, W.W.; Shan, C.J.; Gong, L.Y.; Zhao, S.M. Measurement-induced disturbance near Anderson localization in one-dimensional systems. *J. Phys. B At. Mol. Opt. Phys.* **2014**, *47*, 175503. [CrossRef]
71. Maciá, E. On the nature of electronic wave function in one-dimensional self-similar and quasiperiodic systems. *ISRN Condens. Matter Phys.* **2014**, *2014*, 165943. [CrossRef]
72. Gong, L.; Li, W.; Zhao, S.; Cheng, W. A measure of localization properties of one-dimensional single electron lattice systems. *Phys. Lett. A* **2016**, *380*, 59. [CrossRef]

73. Maciá, E. Spectral classification of one-dimensional binary aperiodic crystals: An algebraic approach. *Ann. Phys. (Berlin)* **2017**, *2017*, 1700079. [CrossRef]
74. Lambropoulos, K.; Simserides, C. Tight-binding modeling of nucleic acid sequences: Interplay between various types of order or disorder and charge transport. *Symmetry* **2019**, *11*, 968. [CrossRef]
75. Diez, E.; Izrailev, F.; Krokhin, A.; Rodríguez, A. Symmetry-induced tunneling in one-dimensional disordered potentials. *Phys. Rev. B* **2008**, *78*, 035118. [CrossRef]
76. Lazo, E.; Diez, E. Conducting and non-conducting transition in dual transmission lines using a ternary model with long-range correlated disorder. *Phys. Lett. A* **2010**, *374*, 3538. [CrossRef]
77. Lazo, E.; Diez, E. Conducting properties of classical transmission lines with Ornstein-Uhlenbeck type disorder. *Phy. Lett. A* **2011**, *375*, 2122. [CrossRef]
78. Lazo, E.; Mellado, F.; Saavedra, E. Rényi entropies of electrical transmission lines with Fibonacci distribution of inductances. *Phys Lett. A* **2012**, *376*, 3423. [CrossRef]
79. Lazo, E.; Diez, E. Phase transition in transmission lines with long-range correlated disorder. *Physica B* **2013**, *419*, 19. [CrossRef]
80. Lazo, E. Generation of intermediate states in diluted disordered direct transmission lines. *Physica B* **2014**, *432*, 121. [CrossRef]
81. Lazo, E.; Humire, F.R.; Saavedra, E. Generation of extended states in diluted transmission lines with distribution of inductances according to Galois sequences: Hamiltonian map approach. *Physica B* **2014**, *452*, 74. [CrossRef]
82. Lazo, E.; Humire, F.R.; Saavedra, E. Disorder-order transitions in diluted and nondiluted direct transmission lines with asymmetric dichotomous noise. *Int. J. Mod. Phys. C* **2014**, *25*, 1450023. [CrossRef]
83. Lazo, E.; Saavedra, E.; Humire, F.R.; Castro, C.E.; Cortés-Cortxexs, F. Localization properties of transmission lines with generalized Thue-Morse distribution of inductances. *Eur. Phys. J. B* **2015**, *88*, 216. [CrossRef]
84. Lazo, E.; Castro, C.E.; Cortés-Cortxexs, F. Overlap amplitude and localization properties in aperiodic diluted and non-diluted direct electric transmission lines. *Phys. Lett. A* **2016**, *380*, 3284. [CrossRef]
85. Lazo, E.; Garrido, A.; Neira, F. The effect of non-linear capacitances in the localization properties of aperiodic dual electric transmission lines. *Eur. Phys. J. B* **2016**, *89*, 249. [CrossRef]
86. Lazo, E. Accurate measurement of the localization properties of electric transmission lines using the overlap amplitude. *Eur. Phys. J. D* **2017**, *71*, 144. [CrossRef]
87. Lazo, E.; Cortés-Cortxexs, F. Disordered mixed transmission lines: Localization behavior. *Eur. Phys. J. Plus* **2019**, *134*, 28. [CrossRef]
88. Lazo, E. Influence of two independent sources with long-range correlated disorder in the localization properties of mixed transmission lines. *Phys.-Low-Dimens. Syst. Nanostruct.* **2019**, *114*, 113628. [CrossRef]
89. Humire, F.R.; Lazo, E. $\mathcal{PT}$-symmetric direct electrical transmission lines: Localization behavior. *Phys. Rev.* **2019**, *100*, 022221. [CrossRef] [PubMed]
90. Lazo, E. Spectral properties of a chain of polyhedra. *Phys. Status Solidi B* **1992**, *169*, 359. [CrossRef]
91. Lazo, E. Mixed Crystal electronic structure of $MS_{3-x}Se_x$. *Phys. Status Solidi B* **1992**, *170*, 463. [CrossRef]
92. Rényi, A. On the foundations of information theory. *Rev. Int. Stat.* **1965**, *33*, 1. [CrossRef]
93. Coffman, V.; Kundu, J.; Wooters, W.K. Distributed entanglement. *Phys. Rev. A* **2000**, *61*, 052306. [CrossRef]
94. Lakshminarayan, A.; Subrahmanyam, V. Entanglement sharing in one-particle states. *Phys. Rev. A* **2003**, *67*, 052304. [CrossRef]
95. Li, H.; Wang, X.; Hu, B. Bipartite entanglement and localization of one-particle states. *J. Phys. A Math. Gen.* **2004**, *37*, 10665. [CrossRef]
96. Albuquerque, S.S.; de Moura, F.A.B.F.; Lyra, M.L. Vibrational modes in harmonic chains with diluted disorder. *Physica A* **2005**, *357*, 165. [CrossRef]
97. de Moura, F.A.B.F.; Viana, L.P.; Frery, A.C. Vibrational modes in aperiodic one-dimensional harmonic chains. *Phys. Rev. B* **2006**, *73*, 212302. [CrossRef]
98. Albuquerque, S.S.; Santos, J.L.L.D.; de Moura, F.A.B.F.; Lyra, M.L. Enhanced localization, energy anomalous diffusion and resonant mode in harmonic chains with correlated mass-spring disorder. *J. Phys. Condens. Matter* **2015**, *27*, 175401. [CrossRef] [PubMed]
99. Sales, M.O.; Alburquerque, S.S.; de Moura, F.A.B.F. Energy transport in a one-dimensional harmonic ternary chain with Ornstein–Uhlenbeck disorder. *J. Phys. Condens. Matter* **2012**, *24*, 495401. [CrossRef] [PubMed]

100. Kaya, T. One-dimensional Anderson model with dichotomic correlation. *Eur. Phys. J. B* **2007**, *60*, 313. [CrossRef]
101. Hilke, M. Localization properties of the periodic random Anderson model. *J. Phys. A Mater. Gen.* **1997**, *30*, L367. [CrossRef]
102. Domínguez-Adame, F.; Gómez, I.; Avakyan, A.; Sedrakyan, D.; Sedrakyan, A. Electron States in a Class of One-Dimensional Random Binary Alloys. *Phys. Status Solidi B* **2000**, *221*, 633. [CrossRef]
103. Deng, W. Anomalous Anderson localization. *Physica B* **2000**, *279*, 224. [CrossRef]